Molecular Pharmacology Fast Forward. Published on July 8, 2020 as DOI: 10.1124/molpharm.120.000003
This article has not been copyedited and formatted. The final version may differ from this version.

Functional impact of the G279S substitution in the adenosine A_1 receptor (A_1R G279S$^{7.44}$), a mutation associated with Parkinson's disease

Shahrooz Nasrollahi-Shirazi, Daniel Szöllösi, Qiong Yang, Edin Muratspahic, Ali-El-Kasaby, Sonja Sucic, Thomas Stockner, Christian Nanoff, Michael Freissmuth

Institute of Pharmacology and the Gaston H. Glock Research Laboratories for Exploratory Drug Development, Center of Physiology and Pharmacology, Medical University of Vienna, Vienna, Waehringerstrasse 13a, Vienna, Austria.

Molecular Pharmacology Fast Forward. Published on July 8, 2020 as DOI: 10.1124/molpharm.120.000003
This article has not been copyedited and formatted. The final version may differ from this version.

Running title: A mutated A_1-receptor associated with Parkinson's disease

author for correspondence:

Michael Freissmuth

Institute of Pharmacology and the Gaston H. Glock Research Laboratories for Exploratory Drug Development, Center of Physiology and Pharmacology, Medical University of Vienna, Vienna, Waehringerstrasse 13a, Vienna, 1090 Austria.

Ph.: +43-1-40160 31371

Fax: +43-1-40160 931300

email: michael.freissmuth@meduniwien.ac.at

Number of text pages: 47

Number of Tables: 1

Number of Figures: 10

Number of references: 78

Abstract word count: 245

Introduction word count: 684

Discussion word count: 1500

Abbreviations:

A_1R, adenosine A_1-receptor; BSA, bovine serum albumine; CPA, N6-cyclopentyladenosine; DPCPX; 8-cyclopentyl-1,3-dipropylxanthine; DMEM, Dulbecco's modified Eagle's medium; FBS, fetal bovine serum; GPCR, G protein-coupled receptor; PBS, phosphate-buffered saline; PMSF, phenylmethylsulfonyl fluoride; SCH23380, 7-chloro-3-methyl-1-phenyl-1,2,4,5-tetrahydro-3-benzazepin-8-ol; XAC, xanthine amine congener

Molecular Pharmacology Fast Forward. Published on July 8, 2020 as DOI: 10.1124/molpharm.120.000003
This article has not been copyedited and formatted. The final version may differ from this version.

Abstract

In medium-size, spiny striatal neurons of the direct pathway, dopamine D_1- and adenosine A_1-receptors are co-expressed and are mutually antagonistic. Recently, a mutation in the gene encoding the A_1-receptor (A_1R-G279S$^{7.44}$) was identified in an Iranian family: two affected off-springs suffered from early onset L-DOPA-responsive Parkinson's disease. The link between the mutation and the phenotype is unclear. Here, we explored the functional consequence of the G279S substitution on the activity of the A_1-receptor after heterologous expression in HEK293 cells. The mutation did not affect surface expression and ligand binding, but changed the susceptibility to heat denaturation: the thermodynamic stability of A_1R-G279S$^{7.44}$ was enhanced by about 2 and 8 K when compared to wildtype A_1-receptor and A_1R-Y288A$^{7.53}$ (a folding-deficient variant used as a reference), respectively. In contrast, the kinetic stability was reduced indicating a lower energy barrier for conformational transitions in A_1R-G279S$^{7.44}$ (73 ± 23 kJ/mol) than in wildtype A_1R (135 ± 4 kJ/mol) or in A_1R-Y288A$^{7.53}$ (184 ± 24 kJ/mol). Consistent with this lower energy barrier, A_1R-G279S$^{7.44}$ was more effective in promoting guanine nucleotide-exchange than wildtype A_1R. We detected similar levels of complexes formed between D_1-receptors and wildtype A_1R or A_1R-G279S$^{7.44}$ by co-immunoprecipitation and bioluminescence resonance energy transfer (BRET). However, lower concentrations of agonist were required for half-maximum inhibition of dopamine-induced cAMP accumulation in cells co-expressing D_1-receptor and A_1R-G279S$^{7.44}$ than in those co-expressing wildtype A_1R. These observations predict enhanced inhibition of dopaminergic signaling by A_1R-G279S$^{7.44}$ *in vivo* consistent with a pathogenic role in Parkinson's disease.

Significance statement

Parkinson's disease is caused by a loss of dopaminergic input from the *substantia nigra* to the caudate nucleus and the putamen. Activation of the adenosine A_1-receptor antagonizes responses elicited by dopamine D_1-receptor. We show that this activity is more pronounced in a mutant version of the A_1-receptor (A_1R-G279S$^{7.44}$), which was identified in individuals suffering from early onset Parkinson's disease.

Molecular Pharmacology Fast Forward. Published on July 8, 2020 as DOI: 10.1124/molpharm.120.000003
This article has not been copyedited and formatted. The final version may differ from this version.

Introduction

The motor symptoms of Parkinson's disease - i.e. brady-/akinesia, rigor, tremor and postural instability - result from a loss of dopamine in the striatum (putamen and caudate nucleus) (Ehringer and Hornykiewicz, 1960). Dopamine is supplied by axonal projections of neurons, which reside in the substantia nigra pars compacta (Hornykiewicz et al., 1973). For reasons, which still remain enigmatic, these neurons are vulnerable and susceptible to degeneration. Hence, the prevalence of Parkinson's disease increases with age (Nussbaum and Ellis, 2003). In most instances, neuronal loss is associated with the accumulation of Lewy bodies and Lewy neurites. These fibrillary aggregates contain α-synuclein (Spillantini et al., 1997) and engulfed organelles (Shahmoradian et al., 2019). α-Synuclein is a small protein, which is largely unstructured in solution, but it adopts a α-helical structure in the presence of highly curved membranes containing acidic phospholipids (Davidson et al., 1998). Thus under physiological conditions, α-synuclein is distributed between two pools, a largely unstructured soluble monomeric form and an α-helical oligomeric from, which associates with synaptic vesicles (Burré et al., 2018). α-Synuclein can also form protofibrils composed of β-sheets (Burré et al., 2018). It is not clear, what triggers β-sheet formation and fibrillary aggregation of α-synuclein *in vivo* (Giasson et al., 1999) but point mutations can enhance aggregation (Narhi et al., 1999); the mutated variants also nucleate fibrillation of wildtype α-synuclein (Wood et al., 1999). Hence, it is not surprising that they act in a dominant manner. These missense mutations in α-synuclein occur in patients suffering from early onset, autosomal dominant Parkinson's disease; in fact, they were the first genetic cause identified in Parkinson's disease (Polymeropoulos et al., 1997; Kruger et al., 1998). However, sporadic Parkinson's disease is substantially more frequent than familial forms. Of the many gene loci, which have been linked to Parkinson's disease over the past two decades (Chang et al., 2017), only a fraction give rise to Mendelian (monogenic) disease, which can be transmitted in an autosomal dominant or recessive form (Zhang et al., 2018). These hereditary forms of Parkinson's disease have nevertheless shed light on the pathogenesis and on genetic risk factors: mutations in signaling pathways including the endocytotic recycling machinery, in mitochondrial regulators and in components of the proteostasis network can lead to Parkinson's disease. Thus, Parkinson's disease is heterogeneous in both,

Molecular Pharmacology Fast Forward. Published on July 8, 2020 as DOI: 10.1124/molpharm.120.000003
This article has not been copyedited and formatted. The final version may differ from this version.

the clinical manifestation and in the underlying cause: in most instances, environmental factors apparently act in combination with a genetic susceptibility (Singleton et al., 2013; Zhang et al., 2018).

Recently, a mutation in the adenosine A_1-receptor, which substituted glycine at the position 279 by serine (A_1R-G279S$^{7.44}$), was identified in a consanguinous Iranian family: two brothers (out of 10 sequenced members) were homozygous for A_1R-G279S$^{7.44}$ and both developed symptoms of Parkinson's disease during their third decade. None of the other heterozygous members were affected. Hence, the A_1R-G279S$^{7.44}$ was proposed as an autosomally recessive transmitted cause of early onset Parkinson's disease (Jaberi et al., 2016). The A_1-receptor is a prototypical GPCR, which is abundantly expressed in the cerebral cortex and the basal ganglia of the human brain (Fastbom et al., 1987). In the striatum, A_1-receptors reside on the postsynaptic membrane of the medium-sized spiny neurons of the direct pathway, where they antagonize the dopamine D_1-receptor mediated signaling (Ferré et al., 1994 & 1997). In addition, A_1-receptors are also present on dopaminergic neurons of the substantia nigra pars compacta, where they reduce dopamine release by presynatic inhibition (Yabuuchi et al., 2006; Borycz et al., 2007). Large prospective studies have shown that consumption of caffeine, which blocks adenosine receptors, protects against the development of Parkinson's disease (Costa et al., 2010; Palacios et al., 2012). Thus, there is circumstantial evidence to posit a pathogenic role of the mutant A_1R-G279S$^{7.44}$ in the development of Parkinson's disease. However, the mechanistic basis remains enigmatic. In this study, we explored the functional consequence of the G279S$^{7.44}$ substitution on the activity of the A_1-receptor after heterologous expression in HEK293 cells. We show that the mutation augmented both, the basal activity of the receptor and it response to agonist-induced activation due to enhanced conformational flexibility. This translated into more potent inhibition of dopamine-induced cAMP accumulation.

Molecular Pharmacology Fast Forward. Published on July 8, 2020 as DOI: 10.1124/molpharm.120.000003
This article has not been copyedited and formatted. The final version may differ from this version.

Materials and Methods

Materials

Cell culture media, DPCPX, buffers, salts and standard reagents were purchased from Sigma Aldrich (St. Louis, MO), fetal bovine serum (FBS) from Biowest (Nuaillé, France), RO 20-1724 (4-(3-butoxy-4-methoxyphenyl)methyl-2-imidazolidone) and XAC from Tocris (Abingdon, UK), adenosine deaminase and Complete™ protease inhibitor cocktail from Roche (Mannhein, Germany), CPA from Abcam (Cambridge, UK), Q5® High-Fidelity 2X Master Mix and NEBuilder® HiFi DNA Assembly from New England BioLabs (Ipswich, MA). The mouse monoclonal anti-HA-antibody immobilized on agarose (A2095) was from Sigma Aldrich (St. Louis, MO), the rabbit monoclonal anti-HA antibody (C29F4) and mouse monoclonal anti-HA antibody (2367) were from Cell Signaling Technology (Cambridge, UK). Mouse monoclonal (M2 clone; F3165) and rabbit polyclonal anti-FLAG antibodies (SC807) were from Sigma Aldrich and from Santa Cruz Biotechnology (Dallas, TX), respectively. Alexa-488 labeled secondary antibody against murine IgG (A32732) for flow cytometry was from Invitrogen (Carlsbad, CA). A fluorescently labelled secondary antibody (donkey anti-rabbit, 926-32213) from Li-Cor (Lincoln, NE) was used for immunoblotting. [^{3}H]Adenine (specific activity 40 Ci/mmol), [^{3}H]DPCPX (specific activity 164 Ci/mmol), [^{3}H]SCH23380 (specific activity 83 Ci/mmol) and [^{35}S]GTPγS (specific activity 1385 Ci/mmol) were purchased from PerkinElmer (Waltham, MA).

The plasmids encoding the human adenosine A_1-receptor harboring a N-terminal FLAG-epitope, the human dopamine D_1-receptor harboring a N-terminal HA-epitope and NanoLuc® luciferase (PNL1.1) were obtained from Sinobiological (Beijing, China), from the cDNA resource center (Bloomsburg University, USA) and from Promega (Fitchburg, WI, USA) respectively. The plasmid encoding the human adenosine A_1-receptor with an eYFP fused to its C-terminus was a kind gift from Rafael Franco (University of Barcelona, Barcelona, Spain). The G279S$^{7.44}$ mutation was introduced into the cDNA of the FLAG- and eYFP-tagged A_1-receptor by site-directed mutagenesis using the QuikChange II site direction mutagenesis kit (Agilent, Santa Clara, CA, USA). The cDNA coding for the D_1-receptor (D_1R) was fused in frame to the N-terminal sequence of NanoLuc® luciferase to generate D_1R-NLuc using NEBuilder® HiFi DNA Assembly from New England

Molecular Pharmacology Fast Forward. Published on July 8, 2020 as DOI: 10.1124/molpharm.120.000003
This article has not been copyedited and formatted. The final version may differ from this version.

Biolabs: for PCR amplification of PNL1.1 vector, standard forward and reverse primers were used: for amplification of the D_1R cDNA, primers were designed to have an additional overhang at their 5' end with the primers used to amplify PNL1.1 vector. The transfection reagent was PEI (linear 25kD polyethylenimine, SantaCruz) and the working stock solution (1mg/ml in water) was kept at 4°C (maximum for 2 weeks). For long term storage up to 12 weeks, the PEI stock solution was kept at -20°C.

Molecular dynamics simulations

The adenosine A1-receptor was simulated using the active form based on the agonist-liganded, G_{i2} protein bound structure (PDB ID: 6D9H; Draper-Joyce et al., 2018) and starting from the inactive conformation based on the antagonist bound structure (PDB ID: 5N2S; Cheng et al., 2017). For either conformation, wildtype and mutant receptor were simulated in the presence of absence of adenosine. The missing loop between TM5 and TM6 (residues 214-222) of the receptor was modeled using MODELLER 9.20 (Shen and Sali, 2006; Web and Sali, 2014) creating 100 structures, which were ranked according to the DOPE score. The best 3 were selected for simulations, the G279S mutation was introduced using Pymol (The PyMOL Molecular Graphics System, version v1.8.4 Schrödinger, LLC). Eight systems were created for each of these three selected structures, i.e. the receptor with an empty binding site (A_1R & A_1R-$G279S^{7.44}$) and with adenosine bound (A_1R.ado & A_1R-$G279S^{7.44}$.ado), each in complex with the G protein (A_1R.G & A_1R $G279S^{7.44}$.G; A_1R.ado.G & A_1R-$G279S^{7.44}$.ado.G) or in the G protein-free state (A_1R & A_1R $G279S^{7.44}$; A_1R.ado & A_1R-$G279S^{7.44}$.ado). Equilibrated membrane embedded systems were created by converting all models into the coarse grain representation of the MARTINI force field (Monticelli et al., 2008; de Jong et al., 2013; Wassenaar et al., 2015), which allowed for fast membrane equilibration. The proteins were embedded into a POPC:cholesterol membrane (70:30 mol%), the simulation box was filled with water and 150 mM NaCl. The coarse grain systems were simulated for 1 μs with the protein structure restrained to avoid conformational changes during membrane equilibration. Next, membrane, water and ions were converted to an all-atom representation (Wassenaar et al., 2014), while the original receptor structure replaced the coarse grain model. Spurious atom overlaps were relaxed using the *membed*

Molecular Pharmacology Fast Forward. Published on July 8, 2020 as DOI: 10.1124/molpharm.120.000003
This article has not been copyedited and formatted. The final version may differ from this version.

procedure (Wolf et al., 2010). In the all atom representation, protein, adenosine and solvent were described using the amber99sb-ildn force field (Lindorff-Larsen et al., 2010), POPC and cholesterol by Slipid (Jämbeck and Lyubartsev, 2012 & 2013). All simulations used GROMACS version 2019.2 (Abraham et al., 2015). The completely assembled systems were energy-minimized and the receptor released in four steps of 2.5 ns each by slowly reducing the position restraints (1000, 100, 10, 1 kJ/mol/nm) acting on the Cα atoms and on adenosine if present. The production runs were carried for 500 ns for each independently assembled system. The temperature was maintained at 310 K using the v-rescale (τ = 0.5 ps) thermostat (Bussi et al, 2007), while separately coupling protein+adenosine, membrane and solvent. Pressure was maintained at 1 bar using the Parrinello-Rahman barostat (Parinello and Rahman, 1981) in a semiisotropic manner and applied a coupling constant of 20.1 ps. Long range electrostatic interactions were described using the smooth particle mesh Ewald method (Darden et al., 1993) applying a cutoff of 0.9 nm. The van der Waals interactions were described using the Lennard Jones potentials applying a cutoff of 0.9 nm. Long range correction for energy and pressure were applied. Coordinates of all atoms were recorded at every 50 ps. Data for figures were extracted with the GROMACS package and processed in R and python scripts using the MD Analysis package, v0.19.2 (Michaud-Agrawal et al., 2011; Gowers et al., 2019). VMD (Humphrey et al., 1996), v1.9.3, and Pymol, v1.8.4, were used for visualization.

Cell culture

HEK293 cells were plated in growth medium (DMEM supplemented with 10% FBS) in 15 cm dishes or 6-well dishes at 37°C in a humidified atmosphere containing 5% CO_2. When the cells were 80% confluent, they were transfected with plasmid(s) of interest using PEI (linear 25kD polyethylenimine, SantaCruz Biotechnology, USA) as a transfection reagent. Briefly, DNA and PEI were mixed at a ratio of 1:3 (w:w) in serum-free DMEM and incubated for 15 min at 22°C. The mixture was then added in a dropwise manner to the dish. If not otherwise indicated, the total amount of DNA and of PEI used for a typical transfection were 11 µg and 33 µg/15 cm dish or 2 µg and 6 µg/well, respectively. All assays were done 24 h after transfection.

Molecular Pharmacology Fast Forward. Published on July 8, 2020 as DOI: 10.1124/molpharm.120.000003
This article has not been copyedited and formatted. The final version may differ from this version.

Membrane preparation

HEK293 cells ($8*10^6$) were seeded in 15 cm dishes. When they were about 80% confluent (about $1.6*10^7$/dish), they were transiently transfected with empty plasmid alone (mock; 11 µg/ dish) or the combination of empty plasmid (5.5 µg/dish) and plasmids encoding the human wild type A_1R (5.5 µg/ dish) or A_1R-G279S$^{7.44}$ (5.5 µg/ dish), which carried a FLAG-epitope on their N-terminus. After 24 h, the monolayer was rinsed with ice-cold phosphate-buffered saline (PBS); subsequently, the cells were mechanically detached with a cell scraper, suspended in 5 ml ice-cold PBS containing 0.5 mM PMSF and harvested by centrifugation at 300 g for 5 min at 4°C. The cell pellet was resuspended in ice-cold hypotonic HME buffer containing 20 mM HEPES.NaOH (pH 7.4), 2 mM $MgCl_2$, 1 mM EDTA 0.1 mM PMSF and the Complete™ protease inhibitor cocktail. Thereafter, the cells were subjected to two freeze-thaw cycles followed by ultrasonication (Sonifier cell disruptor B15, 12 pulses of 0.5 s duration at 50% intensity; Branson Ultrasonics, Danbury, CT). Membranes were pelleted by centrifugation for 15 min at 38,000 g and at 4°C and subsequently resuspended in HME buffer (1ml per 0.2 grams of wet pellet). The protein concentration (about 5 mg/ml) was determined by Coomassie Brilliant Blue binding. Membranes were aliquoted, frozen in liquid nitrogen and stored at –80°C.

Radioligand binding

For [^{3}H]DPCPX saturation and displacement experiments, membranes (2-5 µg/assay) were incubated in 0.1 ml buffer containing 50 mM Tris-HCl (pH 7.4), 2 mM $MgCl_2$, 1 mM EDTA, 0.1 mM GTPγS, 5U/ml adenosine deaminase in the absence and presence of ligands (CPA or XAC) and [^{3}H]DPCPX (covering the range of 0.2 to 8 nM for sturation experiments and ~3 nM for dipslacement experiments) for 30 minutes at 25°C. The reaction was terminated by rapid filtration through GF/C glass fiber filter (Sartorius Stedim, Göttingen, Germany) followed by three washes with ice-cold wash buffer (10 mM Tris.HCl, pH 7.4, 1 mM $MgCl_2$) using a Skatron cell harvester. The radioactivity retained on the filters was measured by liquid scintillation. Nonspecific binding was determined in the presence of 10 µM XAC and represented << 10% of total binding in the K_D concentration range. In saturation experiments, the K_D and B_{max} were determined by subjecting the data to non-linear least-squares curve fitting to the equation for a

Molecular Pharmacology Fast Forward. Published on July 8, 2020 as DOI: 10.1124/molpharm.120.000003
This article has not been copyedited and formatted. The final version may differ from this version.

rectangular hyperbola. In displacement experiments, the IC_{50} was estimated by fitting the data to the equation for a monophasic displacement curve. The K_i was calculated using the Cheng–Prusoff approximation ($K_i = IC_{50}/(1 + [L]/K_{D,L})$. For binding of [^{35}S]GTPγS, membranes (10 µg/assay) were incubated in a total volume of 80 µl containing 50 mM Tris.HCl (pH 7.4), 5 mM $MgCl_2$, 1 mM EDTA, 100 mM NaCl, 10 µM GDP, 5U/ml adenosine deaminase in the absence and presence of CPA or DPCPX for 30 minutes at at 25°C. Thereafter, a solution (20 µL) containing [^{35}S]GTPγS (to ~1 nM final concentration, buffer composition otherwise identical) was added and the incubation was continued for 1 min at 25°C. The incubation was terminated by rapid filtration followed by 3 washes with ich-cold buffer containing 10 mM Tris.HCl (pH 7.4), 1 mM $MgCl_2$, 100 mM NaCl. The radioactivity trapped on the filter was determined as outlined above.

Heat denaturation

Membrane aliquots (5 µg/assay) were incubated in a total volume of 50 µl buffer containing 50 mM Tris-HCl, 2 mM $MgCl_2$, 1 mM EDTA, 5U/ml adenosine deaminase, pH 7.4 at temperatures ranging from 40 to 65° for time intervals ranging from 1 to 120 min. Thereafter, the reactions were placed on ice for 15 min and subsequently incubated in the presence of 3 nM [^{3}H]DPCPX for 1 h on ice in a final volume of 0.1 ml containing the same buffer as described above.

Flow cytometry

HEK293 cells ($0.5*10^6$/well) were seeded into 6-well dishes; when the cells were about 80% confluence ($1*10^6$/well), they were transiently transfected with empty plasmid alone (mock; 2 µg/well) or co-transfected with the combination of empty plasmid (1 or 1.5 µg/well) and plasmid (0.5 or 1 µg/well) encoding the human wildtype or mutant A_1-receptor (A_1R-G279S$^{7.44}$), which carried a FLAG-epitope on their N-terminus. Cells were also co-transfected with plasmids encoding the D_1-receptor (1 µg/well) and wildtype or mutant A_1-receptor (1 µg/well). The transiently transfected HEK293 cells were washed with PBS containing 0.1% BSA, thereafter incubated with PBS containing 1 mM EDTA for 10 min at 37°C to detach the cells and then suspended in ice-cold PBS containing 0.1% BSA to a density of $1*10^6$ cells/ml. The single cell suspension was sequentially incubated with the primary mouse M2 monoclonal anti-Flag antibody (1:2000, Sigma) and the secondary mouse anti-mouse IgG1 antibody conjugated to

Molecular Pharmacology Fast Forward. Published on July 8, 2020 as DOI: 10.1124/molpharm.120.000003
This article has not been copyedited and formatted. The final version may differ from this version.

Alexafluor-488 fluorophore from (1:2000, Invitrogen) for 20 min on ice. Thereafter, cells were pelleted by centrifugation (200 g for 5 min at 4°C), resuspended in PBS containing 0.1% BSA and injected into the flow cytometer (BD FACSCantoTM II; BD Biosciences, Franklin Lakes, USA). Forward versus side scatter was used to identify cell populations and to exclude debris, which were found at the bottom left-hand corner of the FSC vs SSC density plot (not shown). In addition, backgating was used to ensure that debris and dead cells were not included in the analysis. Single parameter histograms were generated to quantify the staining by Alexafluor-488 in the gated area; the specific AUC (area under the curve) was calculated by subtracting the nonspecific AUC obtained from cells transfected with empty vector (mock transfection control).

Immunoprecipitation

HEK293 cells transiently co-expressing the HA-tagged D_1-receptor and the FLAG-tagged wild type or the mutant A_1-receptor (A_1R-G279S$^{7.44}$) were washed thrice with ice-cold PBS, collected in 5 ml PBS containing 0.1 mM PMSF and harvested by centrifugation for 5 min at 300 g and at 4 °C. The cell pellet was suspended in buffer containing 25 mM Tris-HCl (pH 7.4), 2 mM $MgCl_2$, 1mM EDTA, 100 mM NaCl, 1% dodecylmaltoside, 0.1 mM PMSF and EDTA-free Complete™ protease inhibitor cocktail. Cell lysis was achieved by incubation for 1 h with end-over-rotation at 4°C. Thereafter, the solubilized material was retrieved be centrifugation (16,000 g for 15 min at 4°C). Preequilibrated beaded agarose (0.1 ml of a 50% slurry) containing immobilized anti-HA-antibody was added to an aliqout of the lysate (1 mg); the suspension was incubated with end-over-end rotation for 16 h with at 4°C. Samples were centrifuged (1 min at 5,000 g and at 4°C) and washed 3 times. The bound proteins were eluted with 0.1 ml denaturing sample buffer containing 20 mM dithiothreitol by heating at 60°C for 15 min. Thereafter, aliquots (10 µl) were separated by electrophoresis on SDS-polyacrylamide gels; proteins were transferred onto nitrocellulose membrane. Non-specific binding was blocked by incubating the membanes in 25 mM Tris-buffered saline (pH 7.5), 0.1% Tween 20 and 5% bovine serum albumin for 1 h at room temperature. After sequential incubation with anti-FLAG or anti-HA antibodies (1:1000 dilution) and fluorescently labelled Donkey-anti rabbit antibody (1:1000 dilution), the immunoreactivebands were visualized and quantified on an Odyssey Clx infrared fluorescent

Molecular Pharmacology Fast Forward. Published on July 8, 2020 as DOI: 10.1124/molpharm.120.000003
This article has not been copyedited and formatted. The final version may differ from this version.

imaging system (LI-COR Biosciences, Lincoln, NE). Aliquots of the cell lysates (20 µg) were also electrophoretically resolved and transferred to nitrocellulose to verify comparable levels of receptor expression in the starting material. The pertinent blots were also probed with a rabbit antiserum, which recognizes all G protein β-subunits (Hohenegger et al., 1996), to control for equal loading of individual lanes (1:2000 dilution).

Bioluminescence Resonance Energy Transfer (BRET)

HEK293 cells ($0.5*10^6$/well) were seeded into 6-well dishes. When the cells were about 80% ($1*10^6$/well) confluent, the cells were transiently co-transfected with a constant amount of plasmid encoding the human D_1-receptor tagged on its C-terminus with a luciferase the NanoLuc™ (D_1R-NLuc 0.2 µg/well) and increasing amounts (0-1.8 µg/well) of plasmid coding for the wild type (wt A_1R) or the mutant A_1-receptor (A_1R-G279S$^{7.44}$), which were tagged their C-terminus with eYFP. The total amount of plasmid (2 µg/dish) was kept constant by adding the appropriate amount of empty plasmid. After 8 h, cells were detached, seeded into 96 well dishes ($5*10^4$/well) and allowed to adhere for 16 h. After serum withdrawal for 1 h, vehicle (control) or the indicated ligands (i.e. 10 µM CPA, 10 µM dopamine or their combination) and luciferase substrate (furimazine = Nano-Glo®, Promega; 1:200 dilution) were added and bioluminescence was recorded for up to 20 min. BRET readings were taken by simultaneously measuring light emission at 460 nm and at 530 nm in the microplate reader (FlexStation3, Molecular Devices). The BRET unit (BRET) signal was calculated by the ratio of emission at 530 nm (A_1R-YFP) to 460 nm (D_1R-NLuc). Cells expressing BRET donor alone (D_1R-NLuc) were used to determine background. BRET specificity was tested by using human β-arrestin-2 fused at its C-termini to NLuc as a donor and A_1R-YFP as an acceptor, which gave equivalent values to that of the cells expressing donor alone. The net-BRET unit was calculated by subtracting background BRET. The data are presented as milli BRET Unit (mBU = net BRET*1000). Parallel incubations were done with cells solely expressing D_1-receptor tagged with NanoLuc™ and the emission recorded from these cells was subtracted.

Molecular Pharmacology Fast Forward. Published on July 8, 2020 as DOI: 10.1124/molpharm.120.000003
This article has not been copyedited and formatted. The final version may differ from this version.

Accumulation of cAMP

Eight hours after transfection, cells were replated into 6-well plates (3×10^5 cells/well) and incubated for 16 h in DMEM containing 1 µCi/ml [^{3}H]adenine (Waldhoer et al., 1999). Cells were then stimulated with 10 µM dopamine alone or in combination with the indicated concentrations of CPA and DPCPX in a total volume of 1 ml DMEM containing 5 U/ml adenosine deaminase for 20 minutes at 25°C. Thereafter the cells were lysed in 1 ml ice-cold 2.5% perchloric acid containing 100 µM cAMP for 15min on ice. The cell extract was then neutralized with 4.2 M KOH. [^{3}H]cAMP was separated by double column chromatography (Johnson et al., 1994).

Statistical analysis

The first part of the study was exploratory in nature: the pharmacology of the mutant receptor and its expression were characterized without any working hypothesis. Three (coefficient of variation CV ≤25%) to 6 experiments (coefficient of variation CV ≤60%) were considered enough to verify the reproducibility of experimental findings. For experiments examining the hypothesis of constitutive activity (generated by molecular dynamics simualtions and the analysis of thermal stability), the number of experiments was adjusted based on the variation observed: if three experiments did not suffice to show statistical significance, the number of required experiments was estimated with a power calculation (>90% probability of finding a statistically significant difference with $p<0.025$) based on the observed variation. Statistical comparisons were done by paired t-test (for comparison of two groups), by Friedman test (for paired comparison of multiple groups) followed by Holm-Sidak post-hoc testing or by F-test to compare two curves. Transient transfections with plasmids encoding wildtype and mutant receptors and the subsequent measurements were done in parallel. These parallel samples were considered as paired data, because transfection efficiency varied on a day-to-day basis (cf. also Fig. 1D).

Molecular Pharmacology Fast Forward. Published on July 8, 2020 as DOI: 10.1124/molpharm.120.000003
This article has not been copyedited and formatted. The final version may differ from this version.

Results

Heterologous expression of wildtype (A_1R) and mutant adenosine A_1-receptor (A_1R G279S$^{7.44}$)

Many mutations affect the ability of GPCRs to undergo folding in the endoplasmic reticulum (Nanoff and Freissmuth, 2012). In fact a substantial portion of the heterologously expressed wildtype A_1-adenosine receptor is retained and degraded in the endoplasmic reticulum (Pankevych et al., 2003, Kusek et al., 2015). Accordingly, we first examined the impact of the G279S-mutation on receptor levels by transient transfection. Transient rather than stable expression was chosen, because this approach eliminated possible distortions arising from clonal selection of cells. Comparable levels of receptors were detected with the antagonist radioligand (Fig. 1A): in three independent experiments the number of binding competent receptors B_{max} was 5.1 ± 1.1 and 5.9 ±1.3 pmol/mg (means ± S.D) for wildtype A_1R and A_1R-G279S$^{7.44}$, respectively. It is also evident from Fig. 1A that mutant and wildtype receptor did not differ in their affinity for the radioligand (K_D = 1.4 ± 0.3 and 1.5 ± 0.4 nM for wildtype A_1R and A_1R-G279S$^{7.44}$, respectively). Similarly, as exemplified in Fig. 1B for the A_1-selective agonist N6-cyclopentyladenosine (CPA), the G279S$^{7.44}$ mutation did not affect agonist affinity (K_i = 0.4 ± 0.1 and 0.3 ± 0.1 µM for wildtype A_1R and A_1R-G279S$^{7.44}$, respectively). We stress that incubations were done in the presence of GTPγS. In the absence of guanine nucleotides, high-affinity agonist binding sites are expected to exist, which reflect ternary complex formation of agonist, receptor and heterotrimeric G protein. In a buffer devoid of GTPγS, CPA displaced the radioligand with a biphasic curve (not shown). However, the proportion of high-affinity sites was too low to provide reliable estimates for agonist affinity in the ternary complex. This is to be expected in transient transfections with high expression levels: upon membrane preparation, a large fraction of the receptor accumulates in vesicles, where receptor molecules outnumber G proteins. We also used flow cytometry by detecting the receptors via their N-terminal FLAG-epitope tag to verify that equivalent amounts were delivered to the plasma membrane: there was a variation in surface levels in individual transfections, but in paired experiments there was no appreciable difference between wildtype and mutant receptor (Fig. 1C). In addition, the amount of receptors, which was detected on the cells, was related to the amount of plasmid DNA (Fig. 1D).

Molecular Pharmacology Fast Forward. Published on July 8, 2020 as DOI: 10.1124/molpharm.120.000003
This article has not been copyedited and formatted. The final version may differ from this version.

Thermal stability of wildtype and mutant A_1-adenosine receptor

The substitution of G279$^{7.44}$ by serine introduces an additional hydrogen bond donor within transmembrane helix-7 (TM7). We performed molecular dynamics simulations to obtain structural and dynamic insights into the flexibility of wildtype A_1-receptor and the changes caused by the G279S$^{7.44}$ mutation. We used the solved structure of the adenosine-bound human A_1-receptor receptor in complex with G_{i2} as a starting point (Draper-Joyce et al., 2018). Three parallel 500 ns long simulations were carried out for wildtype and mutant receptor, with and without the G protein and in the presence and absence of adenosine. Fig. 2A shows the membrane exposed orientation of the G279S mutation, located in the middle of TM7. The side chain of G279S$^{7.44}$ interacts strongly with the backbone carbonyl of F275$^{7.40}$ (Fig. 2B). A hydrogen bond is much stronger in a hydrophobic environment, where it can povide binding energies up to ~20-25 kJ/mol (Bowie, 2011). The energetic penalty for opening the hydrogen bond is much higher in a hydrophobic environment, because it cannot be replaced by an alternative interaction as it would occur in an aqueous environment. We also analyzed the root mean square fluctuations (RMSF) of the A_1-receptor to quantify the global mobility of the receptor and to detect local changes in protein flexibility (Fig. 2C and D). The global mobility of the A_1-receptor was similar for all systems in complex with G_{i2} (Fig. 2C) and without G_{i2} (Fig. 2D). The pattern of mobility reflects the secondary structure of the receptor: the RMSF declines to low values over transmembrane helices, which reflect their rigidity. In contrast, the loops are much more flexible resulting in local maxima of RMSF. Complex formation with G_{i2} has an ordering effect on the intracellular loop 3 (IL3): the mobility of IL3 is strongly reduced, when interacting with the Gα subunit. The G279S$^{7.44}$ mutation exerts mostly a local effect on TM7 mobility: in the absence of adenosine (i.e. in the apo state), the mobility of TM7 is larger in the mutant than in the wildtype receptor. This is seen in both, the receptor complexed to the G protein (*cf*. brown and dark violet trace in Fig. 2D) and in the absence of the G protein, where the mobility of TM7 is even more pronounced (*cf*. amber and violet trace in Fig. 2D).

Molecular Pharmacology Fast Forward. Published on July 8, 2020 as DOI: 10.1124/molpharm.120.000003
This article has not been copyedited and formatted. The final version may differ from this version.

Hydrogen bonds are an important factor contributing to the forces stabilizing membrane proteins (Bowie, 2000; Stockner et al., 2004). Thus, the additional hydrogen bond in TM7 is predicted to increase thermal stability of the A_1-R-G279S$^{7.44}$. However, TM7 is kinked (cf. Fig. 7A). This bending must be stabilized by helical packing. The additional hydrogen bond introduces a counteracting force, which results in destabilization and hence enhanced flexibility, which is evident from the molecular dynamics simulations, in particular of the G protein-free apo state (amber trace in Fig. 2D). Because of this enhanced flexibility - the mutant receptor also ought to incur a penalty in thermal stability.

These predictions were examined by incubating membranes harboring wildtype and mutant receptors at temperatures ranging from 50 to 63°C. Subsequently, the level of residual binding was determined by incubating the membranes with [^{3}H]DPCPX on ice. If the heat-induced denaturation was allowed to proceed for 10 min, there was a small but consistent difference between wildtype and mutant receptor (Fig. 3A; T_{50} = 55.0 ± 0.6° and 56.7 ± 0.5°C for wildtype A_1R and A_1R G279S$^{7.44}$, respectively). This difference was less evident, if the incubation time was increased to 20 min (Fig. 3B; T_{50} = 53.7 ± 0.5° and 54.3 ± 0.8°C for wildtype A_1R and A_1R G279S$^{7.44}$, respectively). There are two components of protein stability, thermodynamic stability and kinetic stability (Sanchez-Ruiz, 2010): thermodynamic stability refers to the equilibrium between the amount of native functional protein and that of unfolded and partially-unfolded states. It is high, if - at a given temeperature - the equilibrium is tilted in favour of the native protein. Kinetic stability is imparted by a high-energy barrier, which prevents the native state from visiting (partially) unfolded states. This energy barrier corresponds to an activation energy and can therefore be extracted from Arrhenius plots. We examined, which component was affected by the G279S mutation by measuring the time-dependent loss of binding at different temperatures for both, wildtype A_1R (Fig. 3C) and A_1R-G279S$^{7.44}$ (Fig. 3D). As a control, we used A_1R-Y288A$^{7.53}$ (Fig. 2E). This receptor variant has a folding defect, but it can be rescued by pharmacochaperoning (Málaga-Diéguez et al., 2010; Kusek et al., 2015). Accordingly, HEK293 cells were transiently transfected with a plasmid driving the expression of A_1R-Y288A$^{7.53}$ and incubated with 100 µM IBMX (3-isobutyl-1-

Molecular Pharmacology Fast Forward. Published on July 8, 2020 as DOI: 10.1124/molpharm.120.000003
This article has not been copyedited and formatted. The final version may differ from this version.

methylxanthine) for 16 h prior to membrane preparation. This suffices to restore folding and cell surface expression of functionally active A_1R Y288A$^{7.53}$, i.e. the pharmacochaperoned A_1R-Y288A$^{7.53}$ binds the radioligand [^{3}H]DPCPX and engages G_i in a manner comparable to wildtype A_1R (Málaga-Diéguez et al., 2010). In all instances, heat led to a biphasic loss of binding competent receptors (Fig. 3C-E): the curves were adequately described by fitting them to the equation for a biexponential decay. We extracted the rate constants for both, the fast and the slow component to generate Arrhenius plots (Fig. 4A&B). It is evident from Fig. 3C-E that the rate of the slow component increased with rising temperatures. The corresponding Arrhenius plots in Fig. 4A show that this temperature-dependent increase was less pronounced with A_1R-G279S$^{7.44}$ than with the wildtype receptor (*cf*. circles and triangles in Fig. 4A). From the slope of the Arrhenius plot we calculated an activation energy of 135 ± 4 and 73 ± 23 kJ/mol for wildtype A_1R and A_1R-G279S$^{7.44}$, respectively. As predicted, A_1R-Y288A$^{7.53}$ was inactivated at lower temperatures than wild type A_1R or A_1R-G279S$^{7.44}$ (cf. Fig. 3C-E). However, the slope of the Arrhenius plot was actually steeper and hence the activation energy (184 ± 24 kJ/mol) larger than that of A_1R-G279S$^{7.44}$ (*cf*. squares and circles in Fig. 4A). Thus, the G279S$^{7.44}$ mutation reduced the kinetic stability of the receptor.

Regardless of which variant of the A_1-receptor was examined, the rate of the fast component did not show any appreciable dependence on temperature (Fig. 4B), reflecting the low energy barrier of thermodynamic stability (Sanchez-Ruiz, 2010). Plotting the ratio of the slowly denaturing component over the rapidly unfolding component (P_f/P_u) as a function of temperature (1/K) allows for comparing the thermodynamic stability of the receptor variants: it is evident from Fig. 4C that the x-intercept of A_1R-G279S$^{7.44}$ is shifted to the left (i.e. to a higher temperature) of that of wildtype A_1R; the difference of about 2 K is consistent with the difference in melting temperature seen in Fig. 3A. In contrast and as predicted for a folding-deficient mutant, the melting temperature of A_1R-Y288A$^{7.53}$ was lower by some 6.5 K than that of wild type A_1R (cf. squares and triangles in Fig. 4C). Taken together these observations show that A_1R-G279S$^{7.44}$ has an enhanced thermodynamic stability but a reduced kinetic stability, while the reverse is true for A_1R-Y288A$^{7.53}$.

Molecular Pharmacology Fast Forward. Published on July 8, 2020 as DOI: 10.1124/molpharm.120.000003
This article has not been copyedited and formatted. The final version may differ from this version.

Complex formation between the dopamine D_1- and wildtype and mutant A_1-receptors

Adenosine A_1- and dopamine D_1-receptors form heteromeric complexes (Ginés et al., 2000; Rivera-Oliver et al., 2019). When transiently co-expressed with either A_1R or A_1R-G297S$^{7.44}$, D_1-receptors accumulated to comparable levels as assessed by binding of the antagonist radioligand [^{3}H]SCH23380 (B_{max} = 1.2 ± 0.2 and 1.4 ± 0.2 pmol/mg in the presence of wild type A_1R and A_1R-G297S$^{7.44}$, respectively). Similarly, equivalent amounts of receptors were detected by immunoblotting detergent lysates prepared from co-transfected cells (Fig. 5A). We first assessed complex formation by immunoprecipitating the D_1-receptor via its N-terminal HA-tag: in the immunoprecipitate equivalent levels of wild type A_1R and A_1R-G297S$^{7.44}$ were visualized by immunoblotting for the N-terminal Flag-epitope (Fig. 5B).

In addition, we examined complex formation in intact cells by bioluminescence resonance energy transfer between a fixed amount of D_1-receptors, which were C-terminally tagged with a luciferase (NanoLuc™), and increasing amounts of YFP-tagged A_1-receptors. This approach allowed for monitoring complex formation in the absence of receptor activation (Fig. 6A) or after stimulation of the receptors activation by their cognate agonists, i.e. by the A_1-selective agonist CPA (Fig. 6B), dopamine (Fig. 6C) or the combination thereof (Fig. 6D). It is evident that the curves are comparable, i.e. there wasn't any appreciable difference in the interaction of the dopamine receptor with wildtype or mutant A_1-receptor regardless of whether receptors were activated or not (Table 1). This indicates that the receptor heteromers form in a constitutive manner, an interpretation, which is also supported by the co-immunoprecipitation in the absence of receptor activation (Fig. 5B).

Comparison of G_i activation by wild type and mutant A_1-receptor

The analysis of the thermostability suggested that the G279S mutation lowered the energy barrier for conformational changes, because its kinetic stability was lower than that of the wild type receptor (*cf*. Fig. 4A). The RMSF plots summarized in Fig. 2 showed a higher mobility of TM7 in A_1R-G279S$^{7.44}$. We interrogated the molecular dynamics simulations to search for

Molecular Pharmacology Fast Forward. Published on July 8, 2020 as DOI: 10.1124/molpharm.120.000003
This article has not been copyedited and formatted. The final version may differ from this version.

changes in the energy landscape associated with movements of TM7: we quantified the increased mobility of TM7 by measuring the distances between TM3 and TM7 at the extracellular face of the receptor, i.e. the distance between L269$^{7.34}$ and A84$^{3.29}$, and at the site of the mutation site, i.e the distance between T91$^{3.36}$ and H278$^{7.43}$ (Fig. 7A). These measurements captured the changes in stability, dynamics and conformations induced by the G279S$^{7.44}$ mutation. The 2D histogram visualized the movements of TM7 (Fig. 7B) and the associated free energy map (Fig. 7C). It is evident that, in the apo (i.e. ligand-free) state of the receptor, TM7 visits many more positions distant from TM3 than in the adenosine-bound state: this is true for both, the wild type receptor in the presence (cf. first and third 2D-histogram in the top row of Fig. 7B) and absence of G_{i2} (cf. first and third 2D-histogram in the bottom row of Fig. 7B) and for the mutant receptor (cf. corresponding second and fouth 2D-histograms in Fig. 7B). This observation shows that binding of adenosine restrains the movement of TM7. In fact, the distance between TM3 and TM7 becomes shorter at the bottom of the ligand-binding site, as TM7 closes in onto the agonist adenosine. The structural change is visible as a shift in the T91$^{3.36}$-H278$^{7.43}$ distance (y-axis in Fig. 7B & C): in the energy basin, the minimum (indicated by a "x" in Fig. 7C) is located at < 0.9 nm in the presence of adenosine (2D-histograms in the first and second column of Fig. 7C). In contrast, in the absence of adenosine, the most stable distance is larger than 0.9 nm (2D-histograms in the first and second column of Fig. 7C). The most conspicuous difference beween the mutant and the wild type receptor can be appreciated by comparing the energy minima of the apo state in the presence of G_{i2}: in the A_1R G279S$^{7.44}$, the basin of low energy states covers a substantially larger area than in the wildtype receptor (cf. fourth and third 2D-histogram in the top row of Fig. 7C). This observation is consistent with a low energy barrier imparted by the mutation, which allows TM7 and thus the mutant receptor to sample many more conformational states than the wildtype receptor.

In the active state, the receptor has to accommodate the C-terminus of its cognate G protein α-subunit in a cavity, which forms on the intracellular side within the transmembrane bundle. A comparison between the active Gα protein bound conformation and shows large movements of TM5 to create the space that allows for Gα protein binding (cf. Fig. 8A & B). We also examined

Molecular Pharmacology Fast Forward. Published on July 8, 2020 as DOI: 10.1124/molpharm.120.000003
This article has not been copyedited and formatted. The final version may differ from this version.

the effect of G279S$^{7.44}$ mutation on the intracellular face of the receptor by measuring distances between I48$^{2.43}$ and V2035.61 (TM2 – TM5) and between I48$^{2.43}$ and and I232$^{6.33}$ (TM2 – TM6) (highlighted as red lines in Fig. 8B). Simulations starting from the inactive conformation reveal that the size of the cavity is sensitive to the mutation: in the apo state, the G279S$^{7.44}$ mutation (brown trace in Fig. 8C and D) leads to an opening of the binding site fro the Gα protein. In contrast, the wildtype A_1-receptor remains close to its starting structure in the absence of adenosine (red trace in Fig. 8C and D). Fig. 8 E and F show that the bound Gα protein restricts receptor movements, in both the wildtype and the mutant receptor. In contract, the inactive conformation of the A_1-receptor is sensitive to the mutation and the presence of the adenosine ligand. Fig 8, panel C and D show that the mutation leads to an opening of the Gα protein binding site as compared to the wildtype A1-receptor, which remains close to its starting structure in the absence of the adenosine ligand. Addition of the adenosine ligand to the wildtype receptor induces a similar conformational change. A comparison between Fig 8, panel D and F indicate that the time window of the MD simulation of 0.5 μs is not long enough to observe a complete conversion from the inactive to the active conformation.

In most, if not all, GPCRs TM7 is bent; this is also true for the A_1-receptor. This kink is energetically not optimal and used by the receptor to sense agonist binding. The G279S$^{7.44}$ mutation introduces an additional hydrogen bond donor. This ought to stabilize the protein provided that it optimally fits into the structure. However, the traces in figure 8D shows that, in the absence of the G protein, the additional hydrogen bond prefers or needs a different conformation to fulfill its bonding interactions. As a consequence, in the presence of adenosine, helix TM7 of A_1R-G279S$^{7.44}$ oscillates between two conformations (red trace in Fig. 8D).

We surmised that the increased conformational flexibility (Fig. 7C) and the partial opening of the G protein binding site (Fig. 8C & D) ought to translate into more effective agonist-induced G protein activation and/or higher basal - i.e. agonist-independent - activity. This prediction was verified by (i) measuring agonist-induced binding of [^{35}S]GTPγS (Fig. 9A) and (ii) the effect of an

Molecular Pharmacology Fast Forward. Published on July 8, 2020 as DOI: 10.1124/molpharm.120.000003
This article has not been copyedited and formatted. The final version may differ from this version.

inverse agonist on the basal binding of [^{35}S]GTPγS (Fig. 9B) under initial rate conditions (i.e. after 1 min): when stimulated with the agonist CPA at saturating concentrations, the mutant A_1R-G279S$^{7.44}$ caused a larger increase in [^{35}S]GTPγS binding than the wildtype A_1-receptor (Fig. 9A). In contrast, the concentration required for half-maximum stimulation did not differ (EC_{50} = 38 ± 9 nM and 58 ± 19 nM for wildtype A_1R and A_1R-G279S$^{7.44}$, respectively). On average, the basal rate of [^{35}S]GTPγS binding was slightly higher in membranes prepared HEK293 cells transiently expressing A_1R-G279S$^{7.44}$ than those transiently expressing wild type A_1R. Most G protein-coupled receptors have some basal (i.e. constitutive, agonist-independent) activity, which can be blocked by antagonists, which are in most instances inverse agonists (Freissmuth and Schütz 1992; Leff, 1995). This is also true for the A_1-receptor (Freissmuth et al., 1991a). Accordingly, we examined the extent to which a saturating concentration of the antagonist/inverse agonist DPCPX reduced basal [^{35}S]GTPγS binding in membranes from HEK293 cells transiently expressing wildtype A_1R and A_1R-G279S$^{7.44}$. It is evident form Fig. 8B that DPCPX caused a statistically significant inhibition of basal [^{35}S]GTPγS binding to membranes harboring A_1R-G279S$^{7.44}$ by on average 23.4% (95% confidence interval 12.4 to 34.5%). In contrast, there wasn't any appreciable effect of DPCPX on basal [^{35}S]GTPγS binding to membranes harboring wildtype A_1R (on average 1.1% lower than in the absence of DPCPX, 95% confidence interval from 11.8% lower to 9.7% higher). These observations indicate that the constitutive activity of A_1R-G279S$^{7.44}$ is more pronounced than that of the wildtype receptor.

Taken together the data in summarized in Fig. 9 suggested that A_1R-G279S$^{7.44}$ was more effective in promoting nucleotide exchange on cognate G proteins than the wildtype receptor. The A_1-receptor is a prototypical G_i/G_o-coupled receptor, which engages all isoforms of $G\alpha_i$ and $G\alpha_o$ (Freissmuth et al., 1991b; Jockers et al., 1994). The bidirectional regulation of cAMP formation is the major effector pathway, which is regulated in a mutually antagonistic manner by D_1- and A_1-receptors (Ferré et al., 1998). We therefore explored, if wildtype A_1R and A_1R-G279S$^{7.44}$ differed in their ability to inhibit cAMP accumulation induced by the D_1-receptor in transiently co-transfected cells. We first measured dopamine-induced cAMP accumulation in the absence and presence of DPCPX to address the question, whether the different level of

Molecular Pharmacology Fast Forward. Published on July 8, 2020 as DOI: 10.1124/molpharm.120.000003
This article has not been copyedited and formatted. The final version may differ from this version.

constitutive nucleotide exchange activity detected by [^{35}S]GTPγS binding (Fig. 8B) translated into modulation of cAMP production. This was the case: in HEK293 cells co-expressing the D_1-receptor and the mutant A_1R-G279S$^{7.44}$, DPCPX produced a consistent and statistically significant increased the cAMP response to dopamine (by 1.4- ± 0.2-fold; Fig. 10A). In contrast, in HEK293 cells co-expressing the D_1-receptor and the wildtype A_1-receptor, the effect of DPCPX was less pronounced and did not reach statistical significance in spite of the large number of paired observations (increase by 1.2- ± 0.2-fold; Fig. 10A). Similarly, in cells expressing A_1R-G279S$^{7.44}$, the concentration-response curve for CPA was shifted to the left of that seen in cells expressing wildtype A_1R (Fig. 10B; IC_{50} = 2.4 ± 0.5 and 0.9 ± 0.4 nM for wild type A_1-receptor and the mutant A_1R-G279S$^{7.44}$, respectively). While the shift was modest, the difference was consistently observed in paired experiments, where cells were subjected to transient co-transfection with plasmids encoding the D_1-receptor and the wildtype or mutant A_1-receptor (*cf*. inset in Fig. 10B). This difference between wildtype and mutant A1-receptor is consistent with the higher efficacy of the agonist-stimulated A_1R-G279S$^{7.44}$ in promoting guanine nucleotide exchange (Fig. 9A).

Molecular Pharmacology Fast Forward. Published on July 8, 2020 as DOI: 10.1124/molpharm.120.000003
This article has not been copyedited and formatted. The final version may differ from this version.

Discussion

G protein-coupled receptors (GPCRs) represent the largest family of mammalian proteins. Hence their genes collectively occupy a large fraction of the protein coding genome. A survey, which covered 107 GPCRs targeted by approved drugs documented that, on average, an apparently healthy individual harbors 68 non-synonymous coding variations (missense variations) in about one third of these receptors (Hauser et al., 2018). In a database search (www.ensembl.org), we identified 134 missense variations (relative to the reference genome GRCH38.p13) at 96 positions in the coding sequence of the A_1-receptor. Fourteen of these variations (at 12 positions) were found in the 2504 apparently healthy individuals covered by the 1000 genomes project (Auton et al., 2015). However, the only source describing the $G279S^{7.44}$ mutation in the human A_1-receptor is the report by Jaberi et al. (2016), which linked the mutated receptor to early-onset Parkinson's disease. Our experiments were designed to explore the impact of the mutation on the activity of the receptor. Based on our findings, we conclude that the variant $A_1R\text{-}G279S^{7.44}$ has an enhanced conformational flexibility, which translates into a higher basal (i.e. agonist-independent, constitutive) activity and an enhanced agonist-induced response. This conclusion is based on three independent lines of evidence: (i) the kinetic stability of $A_1R\text{-}G279S^{7.44}$ was about 50% lower than that of the wild type receptor. Thus the mutation lowered the energy barrier for conformational transitions and this finding was recapitulated in molecular dynamics simulations. (ii) When probed in the presence and absence of an antagonist/inverse agonist to define the constitutive activity of the receptor, we consistently observed a larger effect of the antagonist/inverse agonist for $A_1R\text{-}G279S^{7.44}$ than for the wild type receptor, regardless of whether guanine nucleotide exchange or by cAMP accumulation was assessed. (iii) The agonist-liganded $A_1R\text{-}G279S^{7.44}$ was more efficacious than the wildtype receptor in catalyzing guanine nucleotide exchange. Accordingly, in cell expressing $A_1R\text{-}G279S^{7.44}$, the agonist concentration-response curve for lowering cAMP levels was shifted to the left of that seen in cells expressing the wild type receptor.

Residues in transmembrane helix 7 (TM7) contribute to the orthosteric binding site of the A_1-receptor; in fact, T270 is the amino acid critical for binding of ligands, which discriminate

Molecular Pharmacology Fast Forward. Published on July 8, 2020 as DOI: 10.1124/molpharm.120.000003
This article has not been copyedited and formatted. The final version may differ from this version.

between the A_1- and the A_{2A}-receptor (Cheng et al., 2017; Glukhova et al., 2017). G279 is about 2.5 helical turns distal to T270. Our experiments rule out that the G279S mutation has indirect effects on the geometry of the ligand binding cavity: both, the A_1-selective antagonist/inverse agonist DPCPX and the agonist CPA bound with similar affinity to the wild type A_1-receptor and to A_1R-G279S$^{7.44}$. Similarly, G279S$^{7.44}$ is about 2.5 helical turns from Y288$^{7.53}$, which is critical for folding of the A_1-receptor in the endoplasmic reticulum: during the conformational search TM7 and the C-terminus must be correctly positioned to allow for emergence of the native conformation (Pankevych et al., 2003; Málaga-Diéguez et al., 2010). The G279S$^{7.44}$ mutation does not interfere with the folding trajectory of the A_1-receptor. This conclusion is based on our observations that equivalent levels of wild type and mutant receptors were found on the cell surface. The A_1-receptor can form homodimers (Gracia et al., 2013) and heteromers, in particular with the D_1-receptor (Ginès et al., 2000; Rivera-Oliver et al., 2019), which allows for their reciprocal, mutually antagonistic modulation (Ferré et al., 1998). The interface in the A_1-/D_1-receptor heteromer is not known, but our observations indicate that the G279S$^{7.44}$ mutation does not affect this interface: wild type and mutant A_1-receptors did not differ in their ability to form complexes with the D_1-receptor regardless of whether the interaction was assessed by co-immunoprecipitation or monitored by BRET.

We used thermal denaturation to probe the conformational flexibility of mutant and wild type A_1-receptors. Heating resulted in irreversible loss of binding. Under our experimental conditions, it was not possible to capture the initial reversible unfolding. Hence, a Lumry-Eyring model is applicable, which in its simplest version posits a two-step process N ⇆ U → D, where N, U and D are the native, reversibly unfolded and irreversibly denatured states, respectively (Lumry and Eyring, 1954). Because the reversibly unfolded state is inaccessible, it is not possible to extract the energy change ΔG (or ΔH) associated with initial unfolding/refolding, i.e. the N ⇆ U transition. However, the rates of denaturation do shed light on the underlying processes. The rapidly denaturing component reflects a fraction of the A_1-receptor, which visits conformational states that are separated by a low energy barrier from the unfolded state. This fraction rather than the rate of denaturation increased with temperature. Hence, the resulting Arrhenius plots

Molecular Pharmacology Fast Forward. Published on July 8, 2020 as DOI: 10.1124/molpharm.120.000003
This article has not been copyedited and formatted. The final version may differ from this version.

were flat. We posit that this rapid rate reflects the thermodynamic stability of the protein. Substitution of G279 by serine introduces an additional hydrogen bond donor into TM7. The most likely acceptor is the backbone carbonyl of F275$^{7.40}$ (Cheng et al., 2017; Glukhova et al., 2017): this conjecture was substantiated by the molecular dynamics simulations. When compared to the wildtype A_1-receptor, the thermodynamic stability of the mutant A_1R-G279S$^{7.44}$ was enhanced: this increase can be accounted for by the extra hydrogen bond donated by the serine residue, which stabilizes TM7. The importance of TM7 for the stability of the receptor is highlighted by the reduced thermodynamic stability of the mutant A_1R-Y288A$^{7.53}$. In contrast, the second component of thermal denaturation proceeded with a slow rate, which was accelerated with increasing temperature resulting in steep Arrhenius plots. This second component reflects the kinetic stability of the receptor. The relationship between thermodynamic and kinetic stability is complex: it may range from a perfect correlation to total independence (Ruiz-Sanchez, 2010). Our observations show that, in the A_1-receptor, thermodynamic stability and kinetic stability are not correlated. This is exemplified by both, A_1R-G279S$^{7.44}$ and A_1R-Y288A$^{7.53}$: the energy barrier, which separated the wildtype A_1-receptor in its ground state from the denatured state(s), was larger than that of A_1R-G279S$^{7.44}$ and smaller than that of A_1R-Y288A$^{7.53}$. We note that the kinetic barrier is substantially smaller in the A_1-receptor (135 kJ/mol) than in rhodopsin (670 kJ/mol; Hubbard 1958; Corley et al., 2011). This difference is not surprising. Rhodopsin supports vision in dim light and thus requires a high thermal barrier to spontaneous conformational transitions (Guo et al., 2014). However, the kinetic barrier for thermal denaturation of the A_1-receptor is larger than that required for productive ternary complex formation (Waldhoer et al., 1999). In the active, G protein-bound state of the A_1-receptor, the ligand-binding site collapses on the agonist (Draper-Joyce et al., 2018). Our molecular dynamics simulations show that this is due to the movement of several helices including TM7, which is facilitated by substituting serine for G279$^{7.44}$. The G279S$^{7.44}$-induced increased flexibility also allows for rationalizing the reduced kinetic stability, the increase in constitutive activity and the enhanced agonist-induced response, because they can all be linked to lower energy barriers between conformational states.

Molecular Pharmacology Fast Forward. Published on July 8, 2020 as DOI: 10.1124/molpharm.120.000003
This article has not been copyedited and formatted. The final version may differ from this version.

In Parkinson's disease, the G279S$^{7.44}$ variant of the A_1-receptor is a rare mutation, because it does not occur in the large set of whole exome sequencing data of the International Parkinson's Disease Genomics Consortium/IPDGC (Blauwendraat et al. 2017). The interpretation is also confounded by the fact that the affected individuals also harbor a mutation (C52Y) on both alleles of the gene encoding PTRHD1 (peptidyl-t-RNA hydrolase domain containing-1) (Elahi, 2018). PTRHD1 is a protein of unknown function, which lacks its eponymous activity: while it binds peptidyl-t-RNA, it does not hydrolyze it (Burks et al., 2016). The role of PTRHD1 in autosomal recessive Parkinson's disease is supported by two additional reports: an adjacent mutation (H53Y) was found in Iranian patients (Khobadadi et al., 2017) and mutations in PTRHD1, which result in truncation of the protein, were identified in African patients (Kuipers et al., 2018). There are two arguments, which support a pathogenic role of A_1R-G279S$^{7.44}$. First, in the striatum there is mutual antagonism between signaling pathways controlled by dopamine and adenosine; in the direct and indirect pathway, A_1- and A_{2A}-receptors counteract the actions of D_1- and D_2-receptors, respectively (Ferré et al., 1994; Ferré et al., 1997; Yabuuchi et al., 2006). Second, while adenosine-induced stimulation of A_1-receptors has been posited to be *a priori* neuroprotective, this may not be the case upon prolonged stimulation (Cunha, 2016; Stockwell et al., 2017). In fact, prolonged stimulation of A_1-receptors promotes the accumulation of α-synuclein in dopaminergic neurons of the substantia nigra and impairs motor control of the animals (Lv et al., 2020). Duplication (Chartier-Darlin et al., 2004) and triplication of the α-synuclein gene (Singleton et al., 2003) results in Parkinson's disease suggesting that increased expression of the protein *per se* suffices to trigger its fibrillation and Lewy body formation. In the brain including the striatum, A_1-receptors are expressed to high levels; nevertheless, they do not have an appreciable constitutive activity (Savinainen et al., 2003). We observed that by comparison with the wildtype A_1-receptor, the mutated variant A_1R-G279S$^{7.44}$ had a measurable constitutive activity. This may translate to a tonic long-term activation of signaling pathways favoring neurodegeneration. Thus, at the very least, the A_1R-G279S$^{7.44}$ may represent a disease-modifying gene, which renders individuals more susceptible to insults that impair the activity of the nigrostriatal dopaminergic neurons.

Molecular Pharmacology Fast Forward. Published on July 8, 2020 as DOI: 10.1124/molpharm.120.000003
This article has not been copyedited and formatted. The final version may differ from this version.

Acknowledgments:

We thank Petra Schaffer and Luka Schmölz for their participation in experiments, which assessed the heat stability of the A_1-receptor and guanine nucleotide exchange, respectively.

Authorship Contributions:

Participated in research design: Freissmuth, Nanoff, Nasrollahi-Shirazi and Stockner

Conducted experiments: Nasrollahi-Shirazi, Szöllösi and Yang

Contributed new reagents or analytic tools: ElKasaby and Sucic and Muratspahic

Performed data analysis: Freissmuth, Nanoff, Nasrollahi-Shirazi, Szöllösi and Stockner

Wrote or contributed to the writing of the manuscript: Freissmuth, Nasrollahi-Shirazi and Szöllösi.

References

Abraham MJ, Murtola T, Schulz R, Páll S, Smith JC, Hess B, and Lindahl E (2015) GROMACS: High performance molecular simulations through multi-level parallelism from laptops to supercomputers. SoftwareX 1-2:19-25

Auton, A., Brooks, L.D., Durbin, R.M., Garrison, E.P., Kang, H.M., Korbel, J.O., Marchini, J.L., McCarthy, S., McVean, G.A., and Abecasis, G.R.; 1000 Genomes Project Consortium (2015) A global reference for human genetic variation. Nature 526:68–74.

Blauwendraat C, Nalls MA, Federoff M, Pletnikova O, Ding J, Letson C, Geiger JT, Gibbs JR, Hernandez DG, Troncoso JC, Simón-Sánchez J, and Scholz SW; International Parkinson's Disease Genomics Consortium (2017) ADORA1 Mutations are not a common cause of Parkinson's disease and dementia with Lewy Bodies. Mov Disord 32:298-299.

Molecular Pharmacology Fast Forward. Published on July 8, 2020 as DOI: 10.1124/molpharm.120.000003
This article has not been copyedited and formatted. The final version may differ from this version.

Borycz J, Pereira MF, Melani A, Rodrigues RJ, Köfalvi A, Panlilio L, Pedata F, Goldberg SR, Cunha RA, and Ferré S (2007) Differential glutamate-dependent and glutamate-independent adenosine A_1 receptor-mediated modulation of dopamine release in different striatal compartments. J Neurochem 101:355-363.

Bowie JU (2000) Understanding membrane protein structure by design. Nat Struct Biol 7:91-94.

Bowie JU (2011) Membrane protein folding: how important are hydrogen bonds? Curr Opin Struct Biol 21:42-49.

Burks GL, McFeeters H, and McFeeters RL (2016) Expression, purification, and buffer solubility optimization of the putative human peptidyl-tRNA hydrolase PTRHD1. Protein Expr Purif 126:49-54.

Burré J, Sharma M, Südhof TC (2018) Cell biology and pathophysiology of α-synuclein. Cold Spring Harb Perspect Med 8:a024091.

Bussi G, Donadio D, and Parrinello M (2007) Canonical sampling through velocity rescaling. J Chem Phys 126:014101.

Chang D, Nalls MA, Hallgrímsdóttir IB, Hunkapiller J, van der Brug M, Cai F; International Parkinson's Disease Genomics Consortium; 23andMe Research Team, Kerchner GA, Ayalon G, Bingol B, Sheng M, Hinds D, Behrens TW, Singleton AB, Bhangale TR, and Graham RR (2017) A meta-analysis of genome-wide association studies identifies 17 new Parkinson's disease risk loci. Nat Genet 49:1511-1516.

Chartier-Harlin MC, Kachergus J, Roumier C, Mouroux V, Douay X, Lincoln S, Levecque C, Larvor L, Andrieux J, Hulihan M, Waucquier N, Defebvre L, Amouyel P, Farrer M, Destée A (2004) α-Synuclein locus duplication as a cause of familial Parkinson's disease. Lancet 364:1167-1169.

Molecular Pharmacology Fast Forward. Published on July 8, 2020 as DOI: 10.1124/molpharm.120.000003
This article has not been copyedited and formatted. The final version may differ from this version.

Cheng RKY, Segala E, Robertson N, Deflorian F, Doré AS, Errey JC, Fiez-Vandal C, Marshall FH, and Cooke RM (2017) Structures of human A_1 and A_{2A} adenosine receptors with xanthines reveal determinants of selectivity. Structure 25:1275-1285.

Corley SC, Sprangers P, and Albert AD (2011) The bilayer enhances rhodopsin kinetic stability in bovine rod outer segment disk membranes. Biophys J 100:2946-2954.

Costa J, Lunet N, Santos C, Santos J, and Vaz-Carneiro A (2010) Caffeine exposure and the risk of Parkinson's disease: a systematic review and meta-analysis of observational studies. J Alzheimers Dis. 20 Suppl 1:S221-238.

Cunha RA (2016) How does adenosine control neuronal dysfunction and neurodegeneration? J Neurochem 139:1019-1055.

Davidson WS, Jonas A, Clayton, DF, and George JM (1998) Stabilization of α-synuclein secondary structure upon binding to synthetic membranes. J Biol Chem 273:9443–9449.

Darden T, York D, and Pedersen L (1993) Particle mesh Ewald: An N· log(N) method for Ewald sums in large systems. J Chem Phys 98:10089-10092.

Draper-Joyce CJ, Khoshouei M, Thal DM, Liang YL, Nguyen ATN, Furness SGB, Venugopal H, Baltos JA, Plitzko JM, Danev R, Baumeister W, May LT, Wootten D, Sexton PM, Glukhova A, and Christopoulos A (2018) Structure of the adenosine-bound human adenosine A_1 receptor-G_i complex. Nature 558:559-563.

de Jong DH, Singh G, Bennett WF, Arnarez C, Wassenaar TA, Schäfer LV, Periole X, Tieleman DP, and Marrink SJ (2013) Improved parameters for the Martini coarse-grained protein force field. J Chem Theory Comput 9:687-697. doi: 10.1021/ct300646g. Epub 2012 Nov 28.

Molecular Pharmacology Fast Forward. Published on July 8, 2020 as DOI: 10.1124/molpharm.120.000003
This article has not been copyedited and formatted. The final version may differ from this version.

Ehringer H, Hornykiewicz O (1960) Verteilung von Noradrenalin und Dopamin (3-Hydroxytyramin) im Gehirn des Menschen und ihr Verhalten bei Erkrankungen des extrapyramidalen Systems [Distribution of noradrenaline and dopamine (3-hydroxytyramine) in the human brain and their behavior in diseases of the extrapyramidal system]. Klin Wochenschr 38:1236-1239.

Elahi E (2018) PTRHD1 and possibly ADORA1 mutations contribute to Parkinsonism with intellectual disability. Mov Disord 33:174.

Fastbom J, Pazos A, Probst A, and Palacios JM (1987) Adenosine A_1 receptors in the human brain: a quantitative autoradiographic study. Neuroscience 22:827-839.

Ferré S, Popoli P, Giménez-Llort L, Finnman U-B, Martínez E, Scotti de Carolis A, and Fuxe K (1994) Postsynaptic antagonistic interaction between adenosine A_1 and dopamine D_1 receptors NeuroReport 6: 73-76

Ferré S, Fredholm BB, Morelli M, Popoli P, and Fuxe K (1997) Adenosine-dopamine receptor-receptor interactions as an integrative mechanism in the basal ganglia. Trends Neurosci 20:482-487.

Ferré S, Torvinen M, Antoniou K, Irenius E, Civelli O, Arenas E, Fredholm BB, and Fuxe K (1998) Adenosine A_1 receptor-mediated modulation of dopamine D_1 receptors in stably cotransfected fibroblast cells. J Biol Chem 273:4718-4724.

Freissmuth M, Selzer E, and Schütz W (1991a) Interactions of purified bovine brain A_1-adenosine receptors with G-proteins. Reciprocal modulation of agonist and antagonist binding. Biochem J 275:651-656.

Freissmuth M, Schütz W, and Linder ME (1991b) Interactions of the bovine brain A_1-adenosine receptor with recombinant G protein alpha-subunits. Selectivity for rGiα-3. J Biol Chem 266:17778-17783.

Giasson BI, Uryu K, Trojanowski JQ, and Lee VM (1999) Mutant and wild type human α-synucleins assemble into elongated filaments with distinct morphologies in vitro. J Biol Chem 274:7619-7622.

Ginés S, Hillion J, Torvinen M, Le Crom S, Casadó V, Canela EI, Rondin S, Lew JY, Watson S, Zoli M, Agnati LF, Verniera P, Lluis C, Ferré S, Fuxe K, and Franco R (2000) Dopamine D1 and adenosine A_1 receptors form functionally interacting heteromeric complexes. Proc Natl Acad Sci U S A 97:8606-8611.

Glukhova A, Thal DM, Nguyen AT, Vecchio EA, Jörg M, Scammells PJ, May LT, Sexton PM, and Christopoulos A (2017) Structure of the adenosine A_1 receptor reveals the basis for subtype selectivity. Cell 168:867-877.

Gowers, RJ, Linke M, Barnoud J, Reddy TJE, Melo MN, Seyler SL, Domanski J, Dotson DL, Buchoux S, Kenney IM, and Beckstein O. (2019) MDAnalysis: a Python package for the rapid analysis of molecular dynamics simulations. United States: N. p., 2019. Web. doi:10.25080/Majora-629e541a-00e.

Gracia E, Moreno E, Cortés A, Lluís C, Mallol J, McCormick PJ, Canela EI, and Casadó V (2013) Homodimerization of adenosine A_1 receptors in brain cortex explains the biphasic effects of caffeine. Neuropharmacology 71: 56–69.

Guo Y, Sekharan S, Liu J, Batista VS, Tully JC, and Yan EC (2014) Unusual kinetics of thermal decay of dim-light photoreceptors in vertebrate vision. Proc Natl Acad Sci U S A 111:10438-10443.

Molecular Pharmacology Fast Forward. Published on July 8, 2020 as DOI: 10.1124/molpharm.120.000003
This article has not been copyedited and formatted. The final version may differ from this version.

Hauser AS, Chavali S, Masuho I, Jahn LJ, Martemyanov KA, Gloriam DE, and Babu MM (2018) Pharmacogenomics of GPCR Drug Targets. Cell 172:41-54.

Hohenegger M, Mitterauer T, Voss T, Nanoff C, and Freissmuth M (1996) Thiophosphorylation of the G protein β-subunit in human platelet membranes: evidence against a direct phosphate transfer reaction to Gα subunits. Mol Pharmacol 49:73-80.

Hornykiewicz O, Lisch HJ, and Springer A (1968) Homovanillic acid in different regions of the human brain: attempt at localizing central dopamine fibres. Brain Res. 11:662-671.

Hubbard R (1958) The thermal stability of rhodopsin and opsin. J Gen Physiol 42:259-280.

Humphrey W, Dalke A, and Schulten K (1996) VMD: Visual molecular dynamics. J Mol Graph 14:33-38.

Jaberi E, Rohani M, Shahidi GA, Nafissi S, Arefian E, Soleimani M, Moghadam A, Arzenani MK, Keramatian F, Klotzle B, Fan JB, Turk C, Steemers F, and Elahi E (2016) Mutation in ADORA1 identified as likely cause of early-onset parkinsonism and cognitive dysfunction. Mov Disord 31: 1004-1011.

Jämbeck JP, and Lyubartsev AP (2012) An extension and further validation of an all-atomistic force field for biological membranes. J Chem Theory Comput 8:2938-2948.

Jämbeck JP, and Lyubartsev AP (2013) Another piece of the membrane puzzle: extending Slipids further. J Chem Theory Comput 9:774-784.

Molecular Pharmacology Fast Forward. Published on July 8, 2020 as DOI: 10.1124/molpharm.120.000003
This article has not been copyedited and formatted. The final version may differ from this version.

Jockers R, Linder ME, Hohenegger M, Nanoff C, Bertin B, Strosberg AD, Marullo S, and Freissmuth M (1994) Species difference in the G protein selectivity of the human and bovine A_1-adenosine receptor. J Biol Chem 269:32077-32084.

Khodadadi H, Azcona LJ, Aghamollaii V, Omrani MD, Garshasbi M, Taghavi S, Tafakhori A, Shahidi GA, Jamshidi J, Darvish H, and Paisán-Ruiz C (2017) PTRHD1 (C2orf79) mutations lead to autosomal-recessive intellectual disability and parkinsonism. Mov Disord 32:287-291.

Kuipers DJS, Carr J, Bardien S, Thomas P, Sebate B, Breedveld GJ, van Minkelen R, Brouwer RWW, van Ijcken WFJ, van Slegtenhorst MA, Bonifati V, and Quadri M (2018) PTRHD1 Loss-of-function mutation in an african family with juvenile-onset Parkinsonism and intellectual disability. Mov Disord 33:1814-1819.

Kusek J, Yang Q, Witek M, Gruber CW, Nanoff C, and Freissmuth M (2015) Chaperoning of the A_1-adenosine receptor by endogenous adenosine - an extension of the retaliatory metabolite concept. Mol Pharmacol 87:39-51.

Krüger R, Kuhn W, Müller T, Woitalla D, Graeber M, Kösel S, Przuntek H, Epplen JT, Schöls L, Riess O (1998) Ala30Pro mutation in the gene encoding α-synuclein in Parkinson's disease. Nat Genet 18:106-108.

Leff P (1995) The two-state model of receptor activation. Trends Pharmacol Sci 16:89-97.

Lumry R, and Eyring H (1954) Conformational changes in proteins. J Phys Chem 58: 110–120.

Lindorff-Larsen K, Piana S, Palmo K, Maragakis P, Klepeis JL, Dror RO, and Shaw DE (2010) Improved side-chain torsion potentials for the Amber ff99SB protein force field. Proteins 78:1950-1958.

Lv YC, Gao AB, Yang J, Zhong LY, Jia B, Ouyang SH, Gui L, Peng TH, Sun S, and Cayabyab FS (2020) Long-term adenosine A1 receptor activation-induced sortilin expression promotes α-synuclein upregulation in dopaminergic neurons. Neural Regen Res. 15:712-723.

Málaga-Diéguez L, Yang Q, Bauer J, Pankevych H, Freissmuth M, and Nanoff C (2010) Pharmaco-chaperoning of the A_1-adenosine receptor is contingent on the endoplasmic reticulum. Mol Pharmacol 77:940-952.

Michaud-Agrawal N, Denning EJ, Woolf TB, and Beckstein O (2011) MDAnalysis: a toolkit for the analysis of molecular dynamics simulations. J Comput Chem 32:2319-2327.

Monticelli L, Kandasamy SK, Periole X, Larson RG, Tieleman DP, and Marrink SJ (2008) The MARTINI coarse-grained force field: extension to proteins. J Chem Theory Comput 4:819-834.

Nanoff C, and Freissmuth M (2012) ER-bound steps in the biosynthesis of G protein-coupled receptors. Subcell Biochem 63:1-21.

Narhi L, Wood SJ, Steavenson S, Jiang Y, Wu GM, Anafi D, Kaufman SA, Martin F, Sitney K, Denis P, Louis JC, Wypych J, Biere AL, Citron M (1999) Both familial Parkinson's disease mutations accelerate α-synuclein aggregation. J Biol Chem 274:9843-9846.

Nussbaum RL, and Ellis CE (2003) Alzheimer’s disease and Parkinson’s disease. N Engl J Med 348:1356–1364.

Palacios N, Gao X, McCullough ML, Schwarzschild MA, Shah R, Gapstur S, and Ascherio A (2012) Caffeine and risk of Parkinson's disease in a large cohort of men and women. Mov Disord 27:1276-1282.

Molecular Pharmacology Fast Forward. Published on July 8, 2020 as DOI: 10.1124/molpharm.120.000003
This article has not been copyedited and formatted. The final version may differ from this version.

Pankevych H, Korkhov V, Freissmuth M, and Nanoff C (2003) Truncation of the A_1-adenosine receptor reveals distinct roles of the membrane-proximal carboxyl terminus in receptor folding and G protein coupling. J Biol Chem 278:30283-30293.

Parrinello M, and Rahman A (1981) Polymorphic transitions in single crystals: A new molecular dynamics method. Journal of Applied Physics 52, 7182-7190.

Polymeropoulos MH, Lavedan C, Leroy E, Ide SE, Dehejia A, Dutra A, Pike B, Root H, Rubenstein J, Boyer R, Stenroos ES, Chandrasekharappa S, Athanassiadou A, Papapetropoulos T, Johnson WG, Lazzarini AM, Duvoisin RC, Di Iorio G, Golbe LI, and Nussbaum RL (1997) Mutation in the α-synuclein gene identified in families with Parkinson's disease. Science 276:2045-2047.

Rivera-Oliver M, Moreno E, Álvarez-Bagnarol Y, Ayala-Santiago C, Cruz-Reyes N, Molina-Castro GC, Clemens S, Canela EI, Ferré S, Casadó V, and Díaz-Ríos M (2019) Adenosine A_1-dopamine D_1 receptor heteromers control the excitability of the spinal motoneuron. Mol Neurobiol 56:797-811.

Sanchez-Ruiz JM (2010) Protein kinetic stability. Biophys Chem 148:1-15.

Savinainen, J.R., Saario, S.M., Niemi, R., Järvinen, T., and Laitinen, J.T. (2003) An optimized approach to study endocannabinoid signaling: evidence against constitutive activity of rat brain adenosine A1 and cannabinoid CB1 receptors. Br. J. Pharmacol. 140, 1451–1459.

Schütz W, and Freissmuth M (1992) Reverse intrinsic activity of antagonists on G protein-coupled receptors. Trends Pharmacol Sci 13:376-380.

Shahmoradian SH, Lewis AJ, Genoud C, Hench J, Moors TE, Navarro PP, Castaño-Díez D, Schweighauser G, Graff-Meyer A, Goldie KN, Sütterlin R, Huisman E, Ingrassia A, Gier Y, Rozemuller AJM, Wang J, Paepe A, Erny J, Staempfli A, Hoernschemeyer J, Großerüschkamp F,

Niedieker D, El-Mashtoly SF, Quadri M, Van IJcken WFJ, Bonifati V, Gerwert K, Bohrmann B, Frank S, Britschgi M, Stahlberg H, Van de Berg WDJ, and Lauer ME (2019) Lewy pathology in Parkinson's disease consists of crowded organelles and lipid membranes. Nat Neurosci 22:1099-1109.

Shen MY, and Sali A (2006) Statistical potential for assessment and prediction of protein structures. Protein Sci. 15:2507-2524.

Singleton AB, Farrer M, Johnson J, Singleton A, Hague S, Kachergus J, Hulihan M, Peuralinna T, Dutra A, Nussbaum R, Lincoln S, Crawley A, Hanson M, Maraganore D, Adler C, Cookson MR, Muenter M, Baptista M, Miller D, Blancato J, Hardy J, and Gwinn-Hardy K (2003) α-Synuclein locus triplication causes Parkinson's disease. Science 302:841.

Singleton AB, Farrer MJ, and Bonifati V (2013) The genetics of Parkinson's disease: progress and therapeutic implications. Mov Disord 28:14-23.

Spillantini MG, Schmidt ML, Lee VM, Trojanowski JQ, Jakes R, and Goedert M (1997) α-Synuclein in Lewy bodies. Nature 388: 839-840.

Stockner T, Ash WL, MacCallum JL, and Tieleman DP (2004) Direct simulation of transmembrane helix association: role of asparagines. Biophys J 87:1650-1656.

Stockwell J, Jakova E, and Cayabyab FS (2017) Adenosine A_1 and A_{2A} receptors in the brain: current research and their role in neurodegeneration. Molecules 22: E676.

Waldhoer M, Wise A, Milligan G, Freissmuth M, and Nanoff C (1999) Kinetics of ternary complex formation with fusion proteins composed of the A_1-adenosine receptor and G protein α-sub-units. J Biol Chem 274:30571-30579.

Wassenaar TA, Pluhackova K, Böckmann RA, Marrink SJ, and Tieleman DP (2014) Going backward: a flexible geometric approach to reverse transformation from coarse grained to atomistic models. J Chem Theory Comput 10:676-690.

Wassenaar TA, Ingólfsson HI, Böckmann RA, Tieleman DP, and Marrink SJ (2015) Computational lipidomics with insane: a versatile tool for generating custom membranes for molecular simulations. J Chem Theory Comput 11:2144-2155.

Webb B, and Sali A (2014) Protein structure modeling with MODELLER. Methods Mol Biol. 1137:1-15.

Wolf MG, Hoefling M, Aponte-Santamaría C, Grubmüller H, and Groenhof G (2010) g_membed: Efficient insertion of a membrane protein into an equilibrated lipid bilayer with minimal perturbation. J Comput Chem 31:2169-2174.

Wood SJ, Wypych J, Steavenson S, Louis JC, Citron M, and Biere AL (1999) α-Synuclein fibrillogenesis is nucleation-dependent. Implications for the pathogenesis of Parkinson's disease. J Biol Chem 274:19509-19512.

Zhang PL, Chen Y, Zhang CH, Wang YX, and Fernandez-Funez P (2018) Genetics of Parkinson's disease and related disorders. J Med Genet 55:73-80.

Yabuuchi K, Kuroiwa M, Shuto T, Sotogaku N, Snyder GL, Higashi H, Tanaka M, Greengard P, and Nishi A (2006) Role of adenosine A_1 receptors in the modulation of dopamine D_1 and adenosine A_{2A} receptor signaling in the neostriatum. Neuroscience 141:19-25.

Molecular Pharmacology Fast Forward. Published on July 8, 2020 as DOI: 10.1124/molpharm.120.000003
This article has not been copyedited and formatted. The final version may differ from this version.

Footnotes:

This work was supported by the doctoral program CCHD (Cell Communication In Health and Disease) funded by a grant from the Austrian Science Fund/FWF (W1205) and by the Medical University of Vienna.

This work is part of a dissertation submitted in partial fulfillment of the requirements of the Ph.D. degree. The authors declare that they have no conflicts of interest with the contents of this article.

Molecular Pharmacology Fast Forward. Published on July 8, 2020 as DOI: 10.1124/molpharm.120.000003
This article has not been copyedited and formatted. The final version may differ from this version.

Figure legends:

Fig. 1**. Binding of the antagonist/**inverse agonist **radioligand [^{3}H]DPCPX (A) and of the agonist CPA (B) to and surface expression of wild type and mutant A_1-receptors (C&D).** ***A: Saturation curve:*** Membranes (5 µg/assay) prepared from HEK293 cells transiently expressing the FLAG-epitope tagged human wild type A_1R (triangle down) or A_1R G279S$^{7.44}$ (full circle) were incubated with the indicated concentrations of [^{3}H]DPCPX for 30 min at 25°C in 0.1 mL buffer. Nonspecific binding was determined in the presence of 10 µM XAC and subtracted. The data are means from duplicate determinations in a representative experiment. The curves were drawn by fitting the data to the equation for a rectangular hyperbola. ***B: Displacement curve***. As described or panel A, membranes (2 - 3 µg/assay) were incubated in the presence of [^{3}H]DPCPX (2.7 nM) in 0.1 mL buffer containing the indicated concentrations of CPA. Data are means ± S.D. from three independent experiments carried out in duplicate with membranes prepared from paired transfections. The curves were drawn by fitting the data to the equation for a monophasic displacement. ***C & D: Flow cytometry histograms and their quantification***. HEK293 cells were transiently transfected with the empty plasmid alone (mock, shaded histogram) or the combination of empty plasmid and plasmid encoding the FLAG-epitope tagged human wildtype A_1R (0.5 or 1 µg/well, black histogram in panel C and full circle in panel D) or A_1R G279S$^{7.44}$ (0.5 or 1 µg/well, red histogram in panel C and triangle down in panel D). The total amount of plasmid (2 µg/disk) was kept constant by adding the appropriate amount of empty plasmid. After 24 h, cells were stained by sequential incubation in the presence of an antibody directed against the FLAG-epitope (1:2000 dilution) and an Alexa-488-conjugated antibody directed against murine IgG1 (1:2000 dilution). The cell-associated fluorescence was quantified by flow cytometry. The histogram shows a representative result from a paired transfection. The results from 4 and 6 paired transfections with 0.5 and 1 µg plasmid DNA encoding wt- or A_1R G279S$^{7.44}$, respectively, are summarized in the spaghetti plot shown in panel D.

Fig. 2. **The G279S mutation enhances TM7 flexibility.** ***A:*** Structural overview of the A_1-receptor. TM7 is highlighted in yellow. The inset shows a zoom-in into the structure of the mutant

Molecular Pharmacology Fast Forward. Published on July 8, 2020 as DOI: 10.1124/molpharm.120.000003
This article has not been copyedited and formatted. The final version may differ from this version.

receptor, which highlights the hydrogen-bond formed between the hydroxyl group of G279S and the backbone of F275$^{7.40}$ (grey sticks). ***B: Frequency distribution of the distance between the carbonyl oxygen of* F275$^{7.40}$ *and the hydrogen of the hydroxyl-group of S279^{7,44}*.** The histogram shows that - in all simulations (i.e., over 3 * 500 ns with 1 ns sampling interval) - this hydrogen-bond opens very rarely regardless of the state (ligand-bound vs. empty apo state; complexed to G protein or free receptor). ***C-D: Root mean square fluctuations (RMSF) of A_1R with and without G protein, respectively.*** RMSF plots show average data of 3 replications, measured with 1 ns temporal resolution. WT and G279S refer to the wildtype and the mutant A_1-receptor, respectively. The apo state corresponds to the empty receptor (binding site devoid of ligand); + G indicates the mutant and wildtype receptor in complex with the G protein G_{i2}. In the apo state (brown and amber traces in C and D, respectively), the upper part of TM7 of A1R-G279S$^{7.44}$ deviates from all other conformations regardless of whether examined with (C) without G protein (D).

Fig. 3**. Heat-induced denaturation of wild type and mutant adenosine A_1-receptors. *A&B*:** Membranes were prepared from HEK293 cells transiently expressing the FLAG-tagged human wild type (wt A_1R, closed triangles), mutant A_1-receptor (A_1R G279S$^{7.44}$, closed circles). Membranes (3-5 µg/assay) were subjected to heat-induced denaturation and incubated for 10 min (A) or 20 min (B) at the indicated temperatures. Thereafter, the membranes were placed on ice. Binding of the [^{3}H]DPCPX (3 nM) was determined for 1 h at 0°C. The curves in A-B were drawn by fitting the data to a three-parameter logistic equation. ***C-E:*** Membranes harboring FLAG-tagged A_1R-Y288A$^{7.53}$ (closed squares) were prepared from transiently transfected HEK293 cells, which had been incubated in the presence of 100 µM IBMX to restore folding and surface expression of the receptor prior to cell lysis. Membranes (3-5 µg/assay for wt A_1R and A_1R-G279S$^{7.44}$; 10- 15 µg/assay for A_1R-Y288A$^{7.53}$) were subjected to denaturation at the indicated temperatures and for the indicated time intervals. Thereafter binding of [^{3}H]DPCPX (3 nM) was determined as outlined for panels A&B. Nonspecific binding was defined in the presence of 10 µM XAC, it was <10% of total binding, did not change with temperature or time and was subtracted. The 100% reference value is binding to control membranes, which were held on ice

Molecular Pharmacology Fast Forward. Published on July 8, 2020 as DOI: 10.1124/molpharm.120.000003
This article has not been copyedited and formatted. The final version may differ from this version.

throughout the experiment. This binding was 10 - 15 fmol/assay. Data are means±S.D. from 3 independent experiments, which were done in parallel. The curves in C-E were drawn by fitting the data to the equation for a biexponential decay.

Fig. 4**. Arrhenius plots for the slow (A) and fast component (B) of heat-induced denaturation and the temperature-dependent change of their ratio (C) for wild type and mutant A_1-adenosine receptors.** ***A&B*****:** The rates of the slow (A) and the fast component (B) were calculated from the individual biexponential decay curves summarized in Fig. 2C-E and their natural logarithm (means ± s.e.m.) plotted as a function of the reciprocal of the absolute temperature. ***C***: The relative proportion of the slowly (P_f) and of the rapidly denaturing (P_u) component were calculated from the individual biexponential decay curves summarized in Fig. 2C-E. The natural logarithms of their ratios (means ± s.e.m.) were plotted as a function of the reciprocal of the absolute temperature. The lines were drawn by linear regression.

Fig. 5. **Co-immunoprecipitation of the wild type adenosine A_1 receptor or the mutant A1R G279S$^{7.44}$ with the dopamine D_1-receptor.** HEK293 cells ($1.6*10^7$/15cm dish) were transiently co-transfected with plasmids encoding the HA-tagged D_1-receptor (5.5 µg/15cm dish) and FLAG-tagged wild type (wt A_1R) or mutant (A_1R-G279S$^{7.44}$) A_1-receptors (5.5 µg/15cm dish). After 24 h cells were detached and lyzed as described in *Materials and Methods* section. An aliquot of the lysate (20 µg/lane) was used to assess the expression of the receptors by immunoblotting with antibodies directed against the epitope tags (panel A). Lysates were also prepared from HEK293 cells subjected to transfection with empty plasmid (lanes labeled mock). The lysates (1 mg) were incubated with beaded agarose containing immobilized HA-antibody. An aliquot (10%) of the immunoprecipitate was resolved by denaturing electrophoresis and transferred to nitrocellulose membranes. The immunoreactive bands of the D_1-receptor (left hand blot in panel B) and of wild type and mutant A_1-receptors (right hand blot in panel B) were visualized by blotting for the HA-and FLAG-epitope tags respectively. Arrows point to the receptor-specific immunoreactivity; the lower bands correspond to the ER-resident core gylcosylated forms of the D_1-receptor and of the A_1-receptor. We note that there are also

Molecular Pharmacology Fast Forward. Published on July 8, 2020 as DOI: 10.1124/molpharm.120.000003
This article has not been copyedited and formatted. The final version may differ from this version.

receptor aggregates, in particular, of the A_1-receptors (immunoreactive bands at about 70 kDa highlighted by an arrow). Data are from a representative experiment, which was replicated four times in independent, paired transfections. The D_1- and A_1-receptor immunoreactivity was quantified by densitometry and the ratio seen in these four experiments is shown in panel C.

Fig 6**. Bioluminescence resonance energy transfer (BRET) between the luciferase tagged dopamine D1-receptor and the wildtype adenosine A_1 receptor or the mutant A_1R G279S$^{7.44}$.** HEK293 cells (1*10^6/well) were transiently co-transfected with a constant amount of plasmid encoding D_1-receptor (D_1R, 1 and 0.2 µg/well for panels A-D and E-H, respectively), which was tagged either on its N-terminus with an HA-epitope (A-D) or on its C-terminus with a luciferase (NanoLuc™) (E-H), and either (1 µg/well; A-D) or increasing amounts (0-1.8 µg/well; E-H) of plasmid coding for the wild type (wt A_1R) or the mutant A_1-receptor (A_1R G279S$^{7.44}$), which were tagged either on their N-terminus with the FLAG-epitope (A-D) on their C-terminus with eYFP (E-H). The total amount of plasmid (2 µg/dish) was kept constant by adding the appropriate amount of empty plasmid. ***A-D: Flow cytometry histograms and their quantification***. After 24 h, cells were detached, divided into two aliquots, which were incubated with murine M2 anti-FLAG antibody (1:2000) or murine anti-HA antibody (1:2000) and then with the secondary anti-mouse IgG antibody conjugated to Alexafluore-488 (1:2000). The resulting receptor-associated immunofluorescence was quantified by flow cytometry as outlined under *Materials and Methods*. ***E-H: BRET recordings in the absence and presence of agonists.*** Eight hours after transfection, cells were seeded into 96 well dishes (5*10^4/well) and allowed to adhere for 15 h. After serum withdrawal for 1 h, vehicle (control) or the indicated ligands (i.e. 10 µM CPA, 10 µM dopamine or their combination) and luciferase substrate (furimazine, 1:200 dilution) were added and bioluminescence was recorded for up to 20 min. Parallel incubations were done with cells solely expressing D_1-receptor tagged with NanoLuc™ and the lumincescence recorded from these cells was subtrated. Data are means ± S.D. from three independent experiments done in parrallel and carried out in duplicate.

Molecular Pharmacology Fast Forward. Published on July 8, 2020 as DOI: 10.1124/molpharm.120.000003
This article has not been copyedited and formatted. The final version may differ from this version.

Fig. 7. **The mutation G279S$^{7.44}$ lowers the free-energy barrier for TM7 to change conformation.** ***A:*** The distances, which were measured during the simulations, are highlighted in the structure of the A_1-receptor. ***B:*** Two-dimensional histogram of the distances between the Cα atoms of T91$^{3.36}$ and H278$^{7.43}$ (x-axes) and of A84$^{3.29}$ and L269$^{7.34}$ (y-axes). ***C*:** Free energy estimate associated with conformational changes in the distances shown in panel B. The minimum position in the free energy basin is indicated by X. Each plot shows the average of 3 independent 500 ns simulations with data points sampled at 1 ns intervals.

Fig. 8. **Geometry of the Gα protein binding cavity of the wildtype adenosine A_1-receptor and of the mutant A1-R-G279S$^{7.44}$.** Snapshots taken at the end of the simulations shows the wildtype A_1-receptor (WT) from the cytoplasmic side with (A) and without (B) bound Gα. The A_1-receptor is represented as white cartoon and TM7 is highlighed in yellow, the bound C-terminal helix of the $G\alpha_{i2}$ protein is shown in transparent red colour. Residues I48$^{2.43}$, I232$^{6.33}$ and V203$^{5.61}$ are shown as sticks. Red lines indicate the distances measured in panel C-F. The inactive receptor is indicated by an asterisk (*). Histograms summarize the frequency at which the indicated distances between the Cα atoms of I48$^{2.43}$ (TM2) and V203$^{5.61}$ (TM5) (C and E) and of I48$^{2.43}$ (TM2) and I232$^{6.33}$ (TM6) (D and F) were observed. Each histogram includes 3 independent simulations of 0.5 µs each. Data points were sampled at 1 ns intervals. The A_1-receptor was simulated using the active form based of the agonist-liganded, G protein bound structure (+ G; PDB ID: 6D9H) and starting from the inactive conformation based on the antagonist bound structure (PDB ID: 5N2S). For either conformation, wildtype (WT) and mutant receptor A1-R-G279S$^{7.44}$ (G279S) were simulated in the absence (apo) and presence of adenosine.

Fig. 9. **[^{35}S]GTPγS binding to membranes prepared from HEK293 cells transiently expressing wildtype or mutant adenosine A_1 receptors.** HEK293 cells were transfected with plasmids driving the expression of the wild type (wt A_1R, triangle down, 5.5 µg/15cm dish) or the mutant (A_1R G279S$^{7.44}$, full circles, 5.5 µg/15cm dish) adenosine A_1 receptor and membranes were

Molecular Pharmacology Fast Forward. Published on July 8, 2020 as DOI: 10.1124/molpharm.120.000003
This article has not been copyedited and formatted. The final version may differ from this version.

prepared as outlined in the legend to Fig. 1A. ***A:*** Membranes (10 µg) were preincubated at 25°C in the absence and presence of the indicated concentrations of the agonist CPA for 30 min; the reaction started by adding [^{35}S]GTPγS to a final concentration of 1 nM and stopped after 1 min by rapid filtration as outlined under *Materials and Methods*. Data are means ± S.D. from three independent experiments (with different membranes from paired transfections) carried out in duplicate. The curves were drawn by fitting the data to the equation describing the hyperbolic concentration-dependent stimulation of a basal activity. The two curves are better described by separate fits rather than by a fit with shared parameters (F-test based on the extra sum of squares-principle; F= 16.03, p=0.0004) because of the difference in the maximal [^{35}S]GTPγS-binding (95% confidence interval 91.5 - 101.3 and 111.5 - 128.1 fmol/mg for wt A_1R and A_1R G279S$^{7.44}$, respectively). ***B:*** The assay was done as described for panel A in the absence (basal) and presence of the antagonist/inverse agonist DPCPX (10 µM). Shown are the results from 6 independent paired transient transfections; each individual experiment is represented by the same symbol. The lines connect basal binding to the corresponding binding in the presence DPCPX to illustrate the consistent inhibition by DPCPX in membranes harboring the mutant receptor A_1R G279S$^{7.44}$ and the absence thereof in membranes harboring the wild type A_1-receptor (wt A_1R). The box plot shows the median and interquartile range; the whiskers correspond to the 95% confidence interval. In membranes carrying A_1R-G279S$^{7.44}$, the difference between basal [^{35}S]GTPγS binding and binding in the presence of DPCPX was statistically significant (p<0.02, Friedman test followed by Holm-Sidak posthoc testing).

Fig 10. **Effect of the A_1-antagonist/inverse agonist DPCPX (A) and of the A_1-agonist CPA (B) on dopamine-induced cAMP accumulation in HEK293 cells co-expressing dopamine D_1 and wild type or mutant adenosine A_1 receptors.** HEK293 cells were transiently co-transfected with plasmids encoding D_1-receptor (D_1R, 5.5 µg/15 cm dish), and wild type A1-receptor (wt A_1R ; 5.5 µg/15 cm dish, triangle down) or themutant A_1R G279S$^{7.44}$ (5.5 µg/15cm dish, full circle). After 8 h, cells were replated into 6-well dishes (0.5*10^6/well) in DMEM medium containing 1 µCi/ml [^{3}H]adenine and incubated for 16 h and subsequently stimulated in medium containing 1 µM dopamine alone or combination of 1 µM dopamine and 10 µM DPCPX (panel A) or increasing

Molecular Pharmacology Fast Forward. Published on July 8, 2020 as DOI: 10.1124/molpharm.120.000003
This article has not been copyedited and formatted. The final version may differ from this version.

concentration of CPA (panel B) for 20 min as outlined under Materials and Methods. ***A:*** Shown are the results from 11 independent paired transient transfections; each individual experiment is represented by the same symbol. The lines connect basal cAMP levels to the corresponding level in the presence DPCPX: addition of DPCPX caused a statistically significant increase in basal cAMP levels in cells expressing A_1R G279S$^{7.44}$ but not in cells expressing wt A_1R (p=0.001 and 0.059, respectively, Friedmann-test fowolled by Holm-Sidak posthoc testing for multiple comparisons). The box plot shows the median and interquartile range; the whiskers correspond to the 95% confidence interval. ***B:*** Data represent means$\pm$SD from four independent experiments and the spaghetti plot in the inset shows the IC_{50} values for wt A_1R and A_1R G279S$^{7.44}$ (paired experiments are indicated by the same symbols). IC_{50}-values differ in a statistically significant manner (p=0.011, t-test for paired data). The curves were drawn by fitting the data to a monophasic inhibition curve. The two curves are better described by separate fits rather than by a fit to a common curve with shared parameters (F-test based on the extra sum of squares-principle; F= 13.57, p=0.0001).

Molecular Pharmacology Fast Forward. Published on July 8, 2020 as DOI: 10.1124/molpharm.120.000003
This article has not been copyedited and formatted. The final version may differ from this version.

Table 1.

Complex formation between dopamine D_1-receptor and wildtype adenosine A_1-receptor or the mutant A_1R $G279S^{7.44}$

Incubation	**A_1-receptor variant**	**$BRET_{50}$ (μg A_1R plasmid)**	**Maximum BRET signal (mBRET)**
Control	wildtype A_1R	0.6±0.1	177±9
	A_1R $G279S^{7.44}$	0.5±0.1	160±30
CPA (10 μM)	wildtype A_1R	0.9±0.2	218±64
	A_1R $G279S^{7.44}$	0.9±0.2	202±37
dopamine (10 μM)	wildtype A_1R	0.7±0.1	207±27
	A_1R $G279S^{7.44}$	0.8±0.1	190±28
CPA & dopamine (10 μM each)	wildtype A_1R	1.1±0.3	226±82
	A_1R $G279S^{7.44}$	1.4±0.6	229±23

$BRET_{50}$ refers to the amount of plasmid encoding wild type or mutant adenosine A_1-receptor giving half-maximum bioluminescence resonance energy transfer; maximum BRET is the response estimated at saturation. The values (means ± S.D.) were calculated by fitting the data from 3 independent experiments (summarized in Fig. 4) to the equation of a rectangular hyperbola.

Molecular Pharmacology Fast Forward. Published on July 8, 2020 as DOI: 10.1124/molpharm.120.000003
This article has not been copyedited and formatted. The final version may differ from this version.

Fig. 1

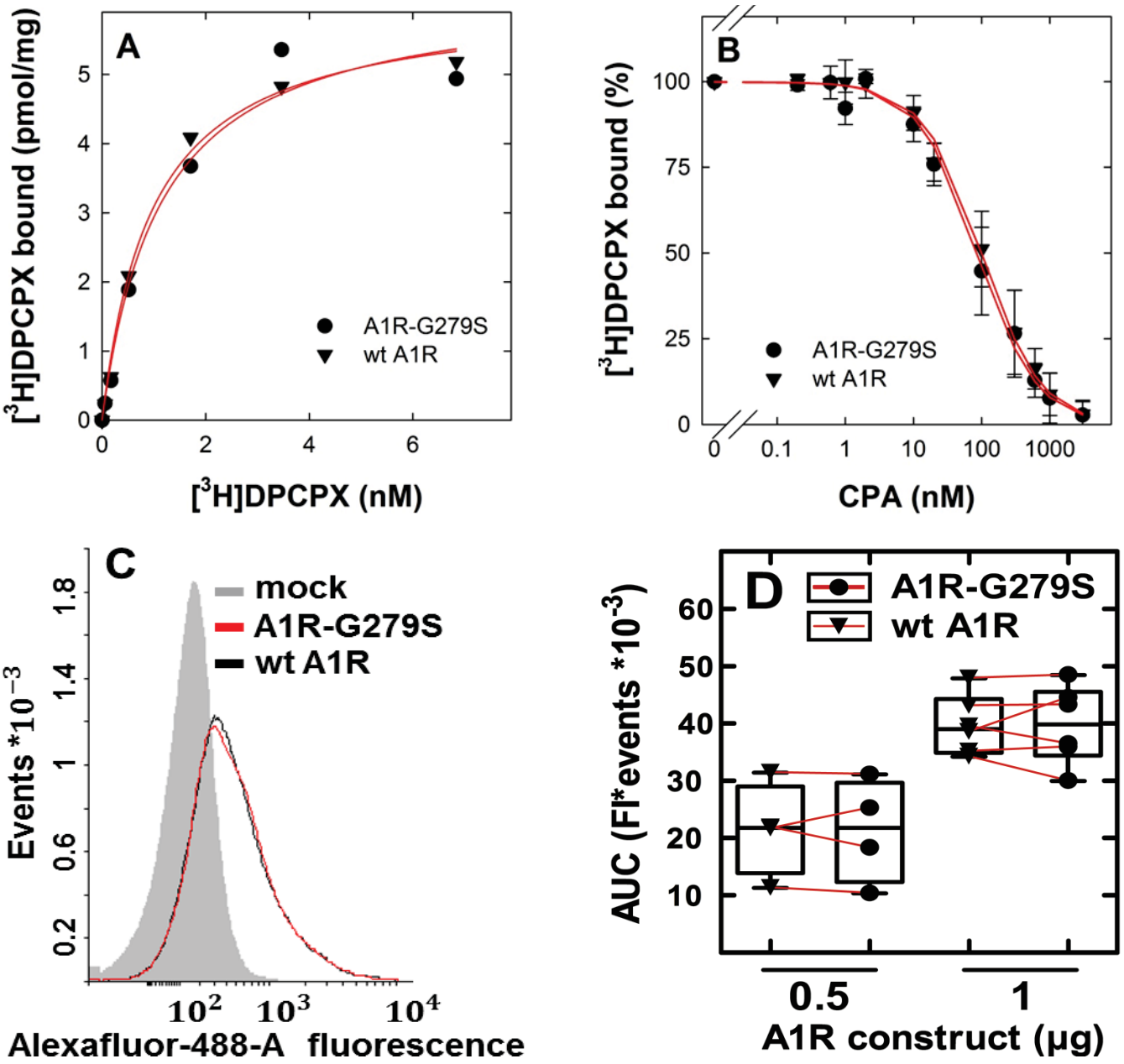

Molecular Pharmacology Fast Forward. Published on July 8, 2020 as DOI: 10.1124/molpharm.120.000003
This article has not been copyedited and formatted. The final version may differ from this version.

Fig. 2

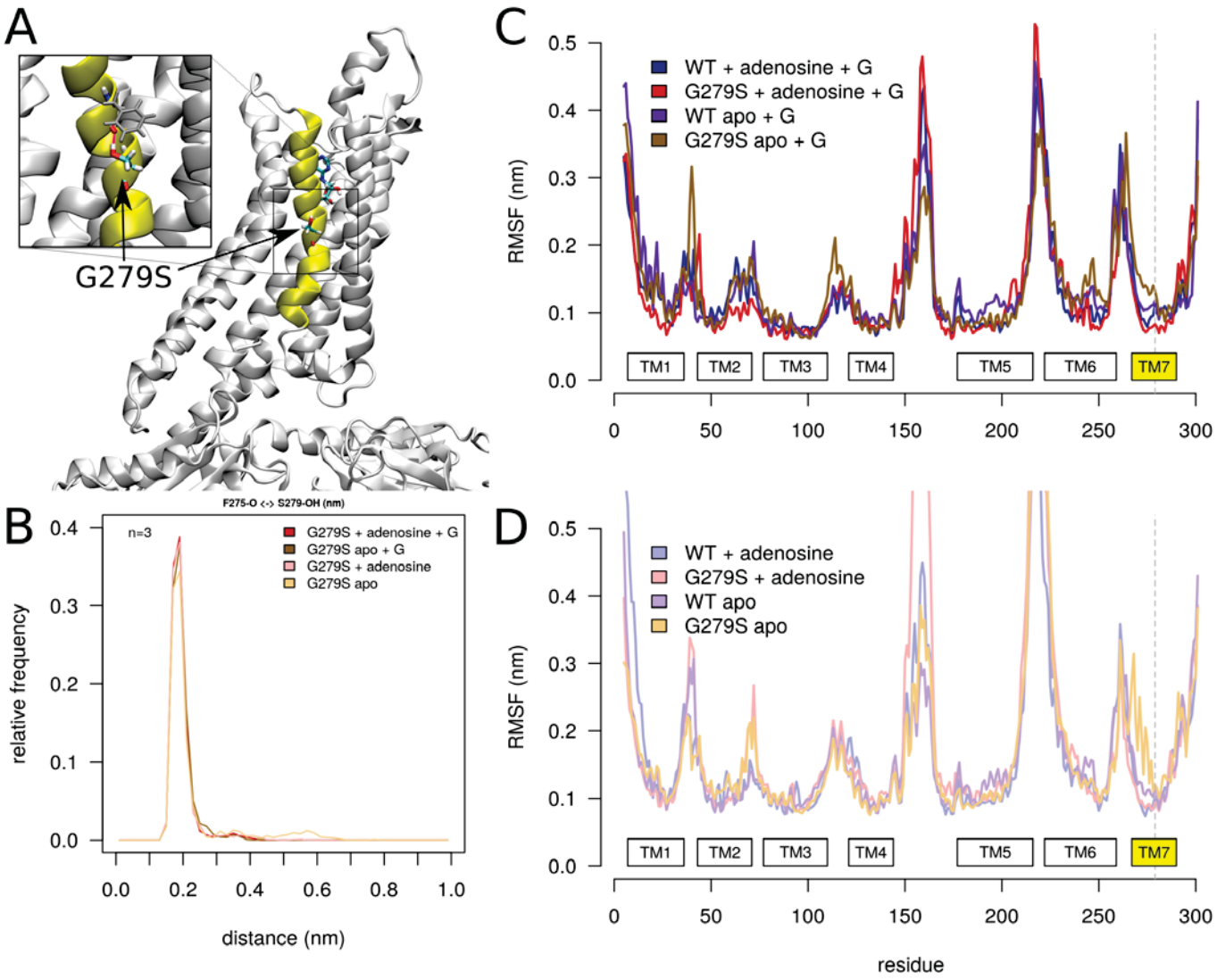

Molecular Pharmacology Fast Forward. Published on July 8, 2020 as DOI: 10.1124/molpharm.120.000003
This article has not been copyedited and formatted. The final version may differ from this version.

Fig. 3

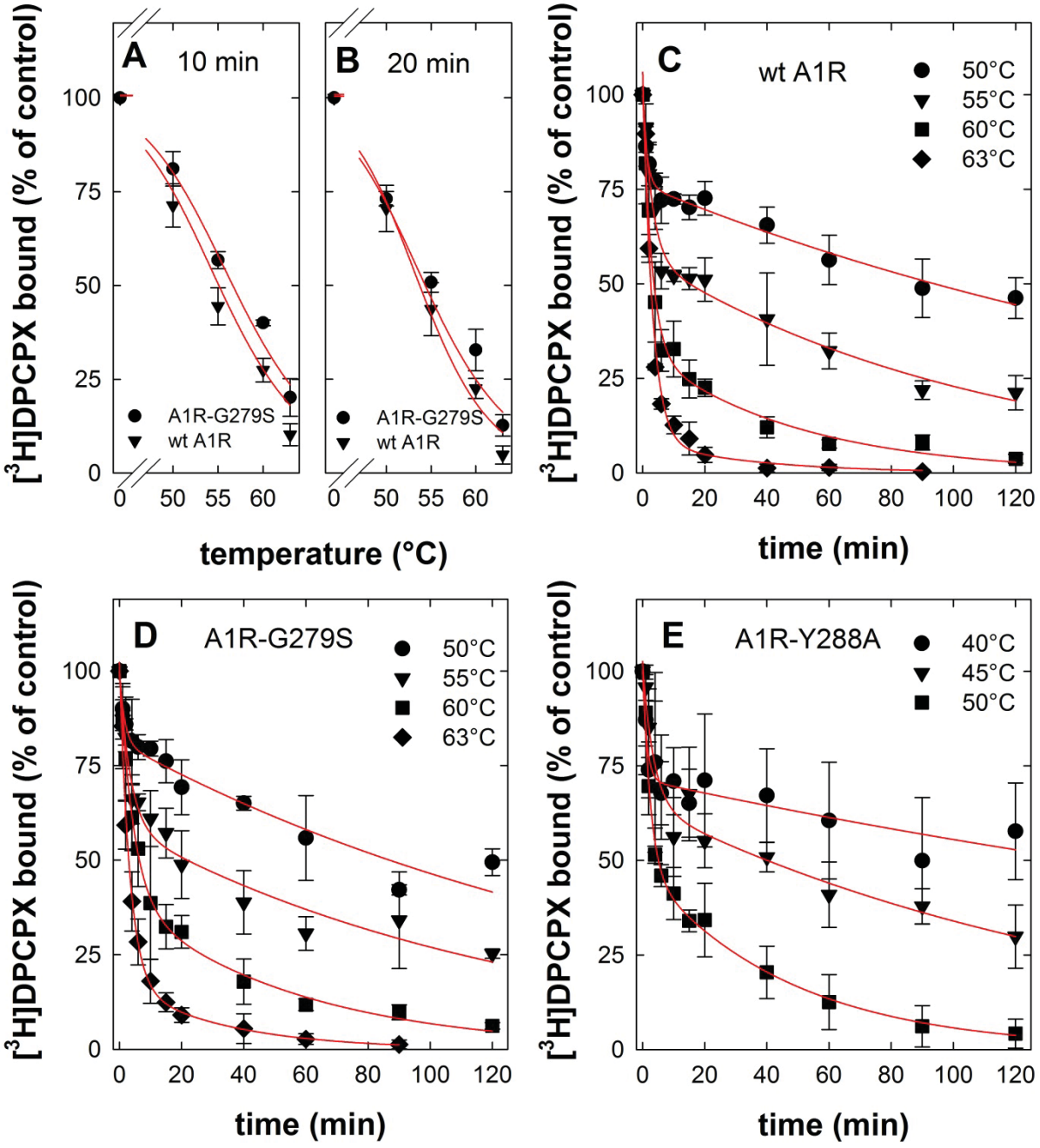

Molecular Pharmacology Fast Forward. Published on July 8, 2020 as DOI: 10.1124/molpharm.120.000003
This article has not been copyedited and formatted. The final version may differ from this version.

Fig. 4

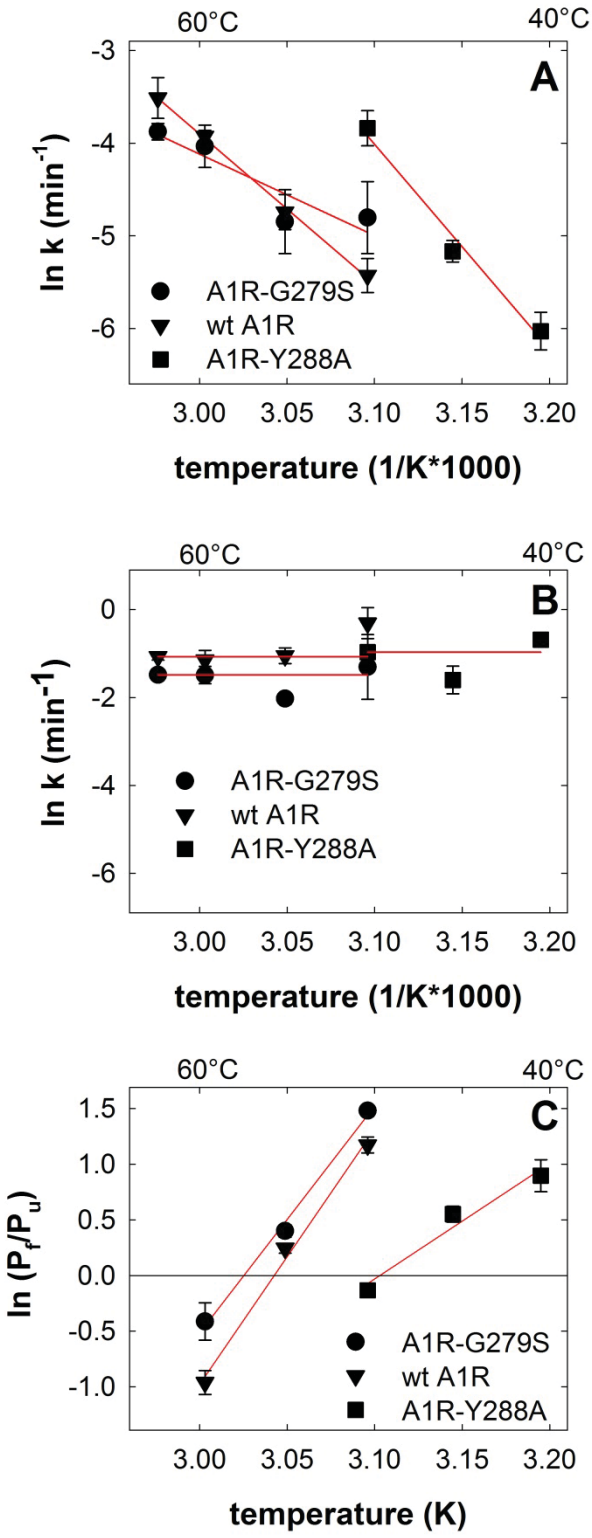

Molecular Pharmacology Fast Forward. Published on July 8, 2020 as DOI: 10.1124/molpharm.120.000003
This article has not been copyedited and formatted. The final version may differ from this version.

Fig. 5

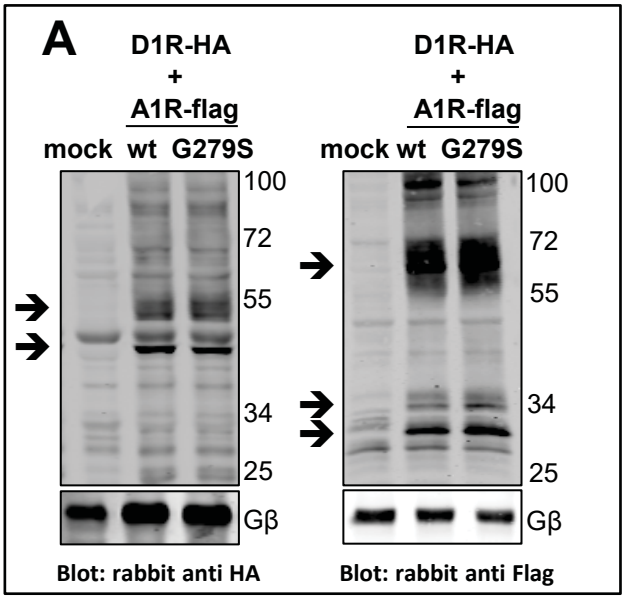

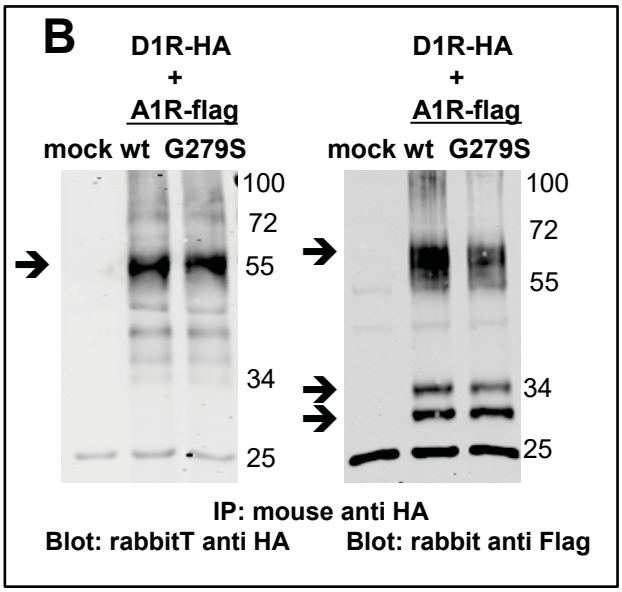

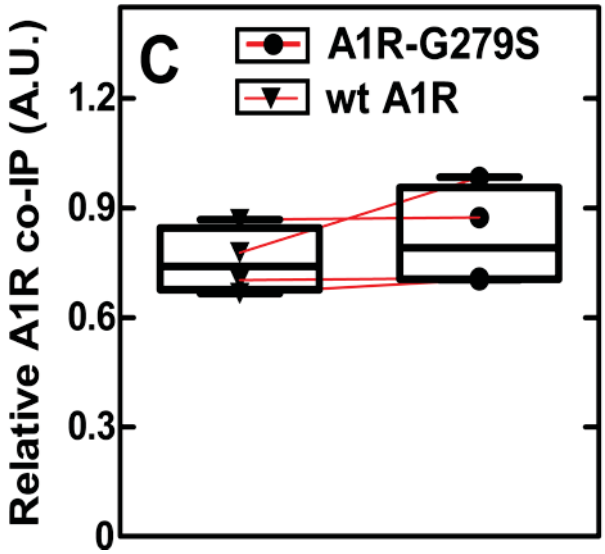

Molecular Pharmacology Fast Forward. Published on July 8, 2020 as DOI: 10.1124/molpharm.120.000003
This article has not been copyedited and formatted. The final version may differ from this version.

Fig. 6

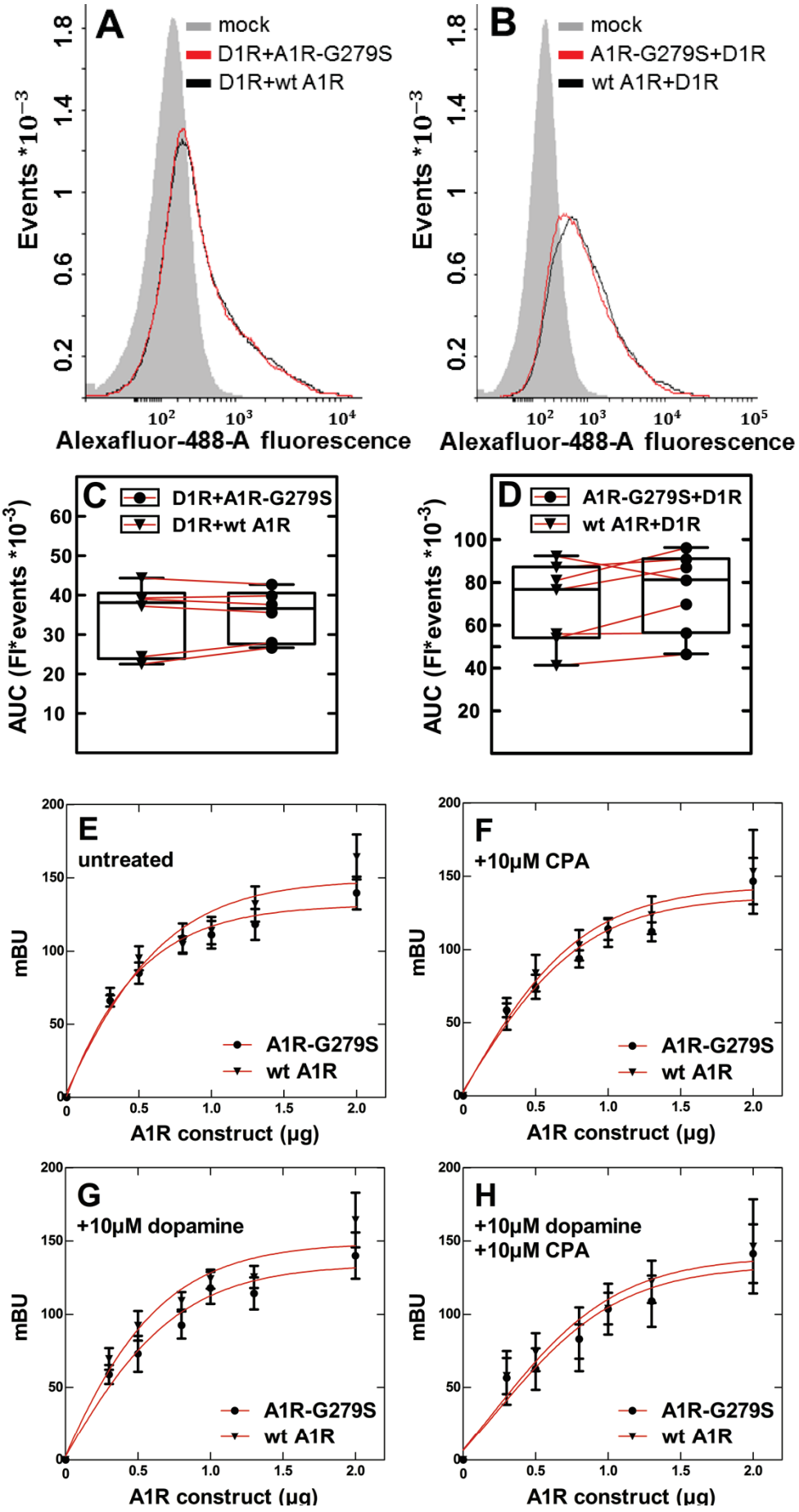

Molecular Pharmacology Fast Forward. Published on July 8, 2020 as DOI: 10.1124/molpharm.120.000003
This article has not been copyedited and formatted. The final version may differ from this version.

Fig. 7

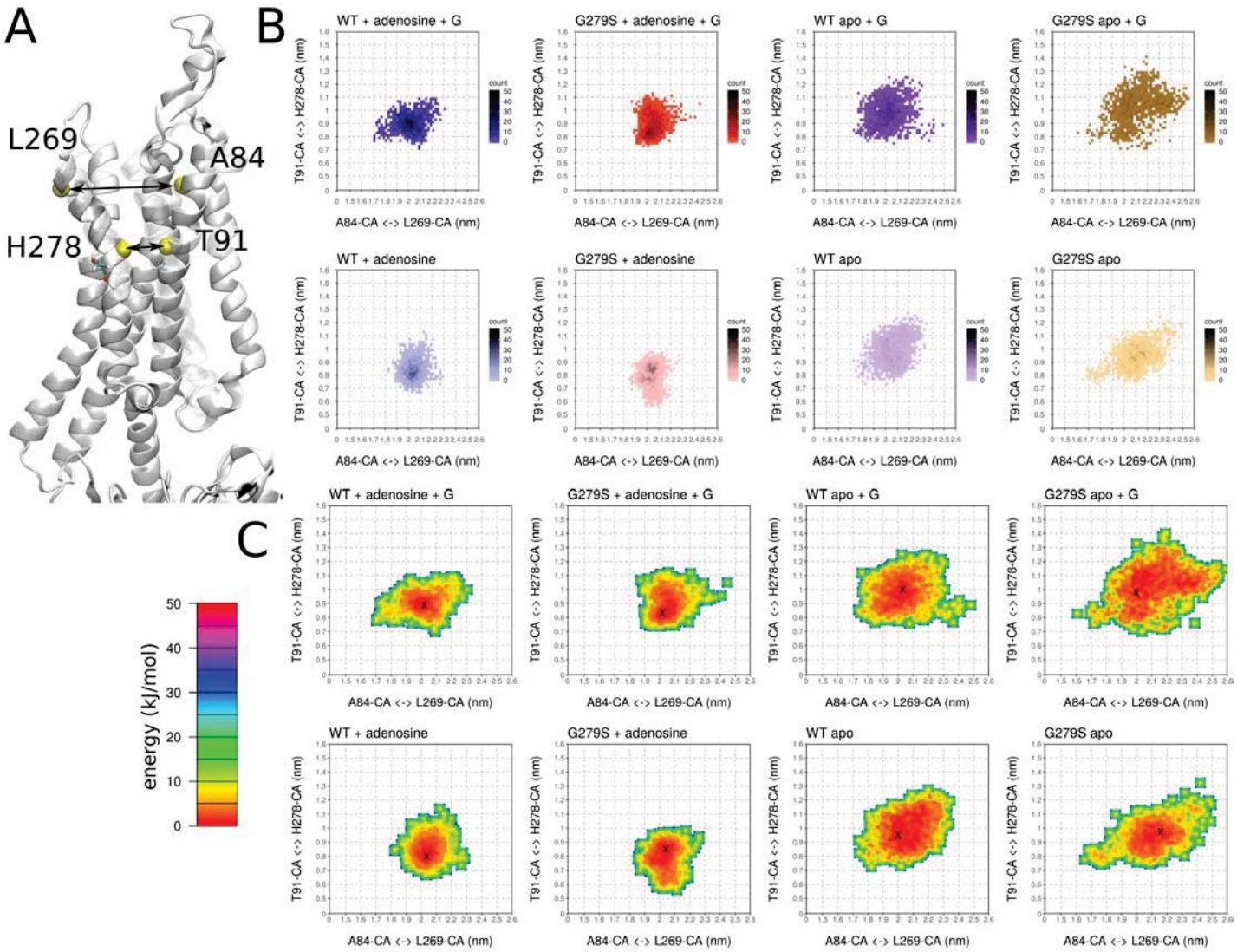

Molecular Pharmacology Fast Forward. Published on July 8, 2020 as DOI: 10.1124/molpharm.120.000003
This article has not been copyedited and formatted. The final version may differ from this version.

Fig. 8

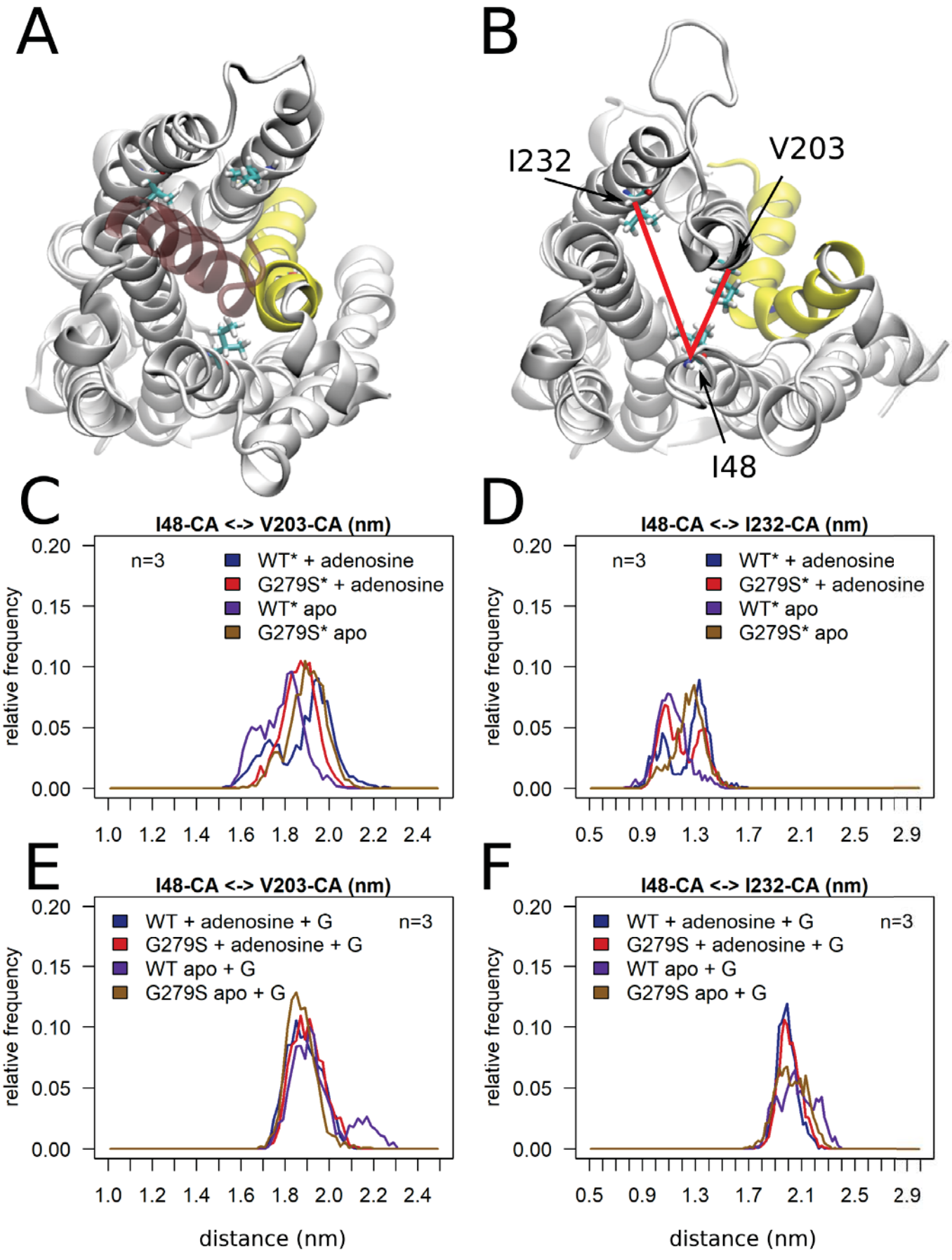

Fig. 9

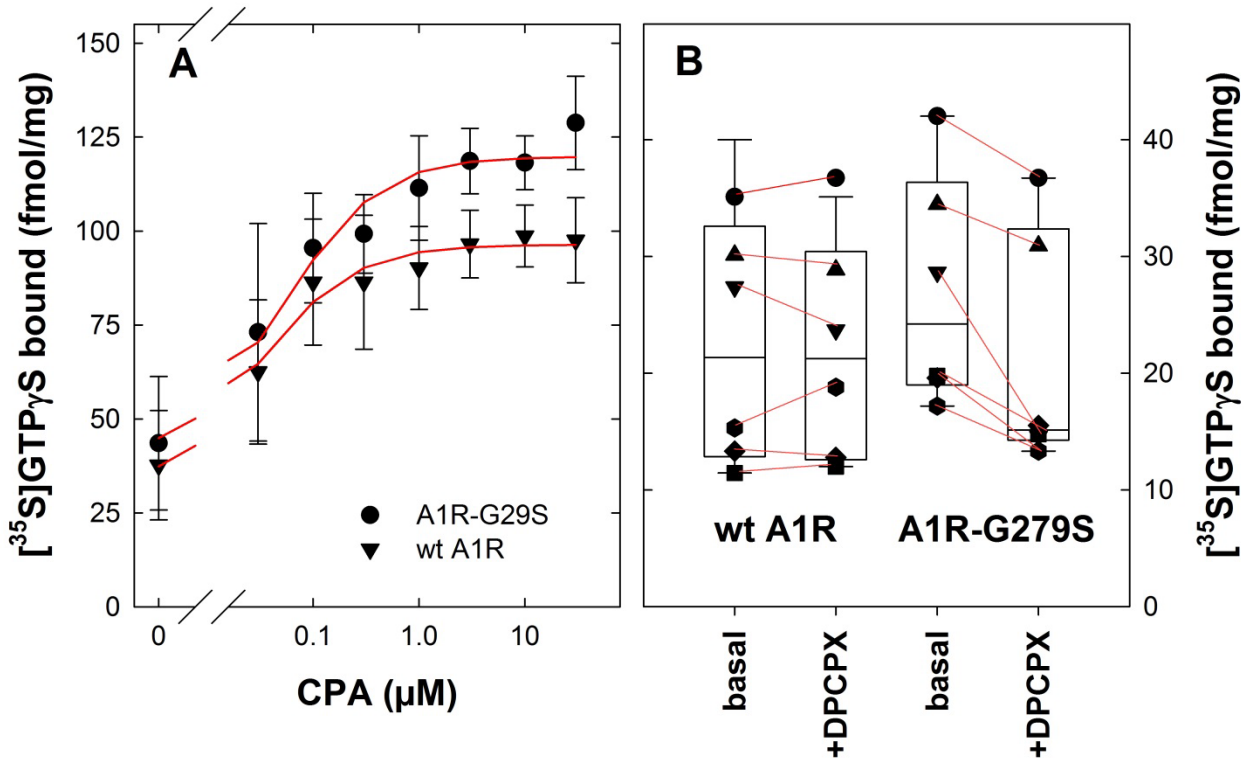
A
B
[35S]GTPγS bound (fmol/mg)
150
125
100
75
50
25
0
A1R-G29S
wt A1R
0
0.1
1.0
10
CPA (μM)
40
30
20
10
0
wt A1R
A1R-G279S
basal
+DPCPX
basal
+DPCPX

Molecular Pharmacology Fast Forward. Published on July 8, 2020 as DOI: 10.1124/molpharm.120.000003
This article has not been copyedited and formatted. The final version may differ from this version.

Fig. 10